

Martin O'Malley, *Governor*
Anthony G. Brown, *Lt. Governor*



James T. Smith, Jr., *Secretary*
Melinda B. Peters, *Administrator*

STATE HIGHWAY ADMINISTRATION

RESEARCH REPORT

AUTOMATED LOW-COST AND REAL-TIME TRUCK PARKING INFORMATION SYSTEM

*ALI HAGHANI
SINA FARZINFARD
MASOUD HAMED
FARSHAD AHDI
MEHDI KALANTARI KHANDANI*

UNIVERSITY OF MARYLAND, COLLEGE PARK

Project number SP209B4M

FINAL REPORT

November 2013

The contents of this report reflect the views of the author who is responsible for the facts and the accuracy of the data presented herein. The contents do not necessarily reflect the official views or policies of the Maryland State Highway Administration. This report does not constitute a standard, specification or regulation.

Technical Report Documentation Page

| | | | |
|--|---|---|-----------|
| 1. Report No. MD-13- SP209B4M | 2. Government Accession No. | 3. Recipient's Catalog No. | |
| 4. Title and Subtitle Automated Low-Cost and Real-Time Truck Parking Information System | | 5. Report Date November 2013 | |
| | | 6. Performing Organization Code | |
| 7. Author/s Ali Haghani, Sina Farzinfard, Masoud Hamed, Farshad Ahdi, Mehdi Kalantari Khandani | | 8. Performing Organization Report No. | |
| 9. Performing Organization Name and Address University of Maryland 1179 Glenn L. Martin Hall College Park, MD 20742 | | 10. Work Unit No. (TRAIS) | |
| | | 11. Contract or Grant No. SP209B4M | |
| 12. Sponsoring Organization Name and Address Maryland State Highway Administration Office of Policy & Research 707 North Calvert Street Baltimore MD 21202 | | 13. Type of Report and Period Covered Final Report | |
| | | 14. Sponsoring Agency Code (7120) STMD - MDOT/SHA | |
| 15. Supplementary Notes | | | |
| 16. Abstract <p>In this project an automated real-time parking information system was developed to improve truck-parking safety through efficient gathering and disseminating information regarding the use of existing parking capacity. The system consists of four main components: sensing, data collection, data processing and user interface (UI). A pilot deployment was conducted on an SHA's truck parking facility located on I-95 northbound prior to MD 32. During the testing period of January 6 through 14, 2013, 1,239 events were detected by the system. Each event refers to any truck arrival or departure activity in a spot. The average overall detection error was 3.75 percent and the maximum error was 5 percent. The error rate can potentially be reduced by using more sensors at each spot and using repeaters to avoid signal blockages.</p> <p>Unlike imagery based methods, magnetic truck detection is completely anonymous and thus privacy of drivers is not compromised. It is also independent of parking layout. In addition to providing real-time parking availability information to the truckers, analysis of historical data for each spot and for the parking facility as a whole can reveal dynamics of events and facilitate efficient operations.</p> | | | |
| 17. Key Words Sensor, Wireless, Truck, Parking | | 18. Distribution Statement: No restrictions This document is available from the Research Division upon request. | |
| 19. Security Classification (of this report) None | 20. Security Classification (of this page) None | 21. No. Of Pages 74 | 22. Price |

Form DOT F 1700.7 (8-72) Reproduction of form and completed page is authorized.

Table of Contents

| | | |
|-------|---|----|
| 1 | Introduction | 1 |
| 2 | System Design and Architecture | 10 |
| 2.1 | Sensing Component | 11 |
| 2.1.1 | Sensor | 12 |
| 2.1.2 | Power Supply | 14 |
| 2.1.3 | RF Antenna | 17 |
| 2.1.4 | Microcontroller | 21 |
| 2.1.5 | Enclosure Design | 21 |
| 2.2 | Collecting Component | 22 |
| 2.2.1 | Microcontroller | 23 |
| 2.2.2 | RF Antenna | 23 |
| 2.2.3 | Cellular Broadband Transceiver | 24 |
| 2.2.4 | Camera | 26 |
| 2.2.5 | Power Supply | 27 |
| 2.3 | Processing Component | 28 |
| 2.4 | User Interface Component | 30 |
| 3 | System Deployment on UMD Campus | 32 |
| 4 | Signal Processing and Results | 35 |
| 4.1 | Magnetic Sensors' Output Data and Calibration | 36 |
| 4.2 | Magnetic Field Distribution for Vehicles | 41 |
| 4.3 | Temperature Drift and Magnetic Cross Interference | 44 |
| 4.4 | Processing Algorithm | 50 |
| 4.5 | Testing and Modifications | 57 |
| 5 | Distributed Data Processing | 60 |
| 6 | Conclusions | 71 |
| 7 | References | 73 |

Table of Figures

| | |
|--|----|
| Table 1-1: Types of sensors used for parking application..... | 4 |
| Figure 1-1: Relative cost comparison for different types of sensors..... | 7 |
| Figure 1-2: Schematic of parking information system design | 9 |
| Figure 2-1: System architecture..... | 10 |
| Figure 2-2: Sensing component | 11 |
| Figure 2-3: Sensitivity of Magnetic Sensors..... | 13 |
| Figure 2-4 : Experiment results for power consumption..... | 16 |
| Figure 2-5: Setup to measure power consumption..... | 17 |
| Figure 2-6: Experiment setup for testing link quality and packet loss..... | 19 |
| Figure 2-7: Results of LQI and packet loss experiments | 19 |
| Figure 2-8: Directional tests on connectivity performance | 20 |
| Figure 2-9: Antenna types | 21 |
| Figure 2-10 Enclosure Design | 22 |
| Figure 2-11 Block diagram of data collector..... | 23 |
| Figure 2-12 : Operational flow for cellular broadband transceiver (CBT)..... | 25 |
| Figure 2-13 : Image sample captured and time stamped by the collecting component..... | 26 |
| Figure 2-14 : Power supply sub-system of the collecting component..... | 27 |
| Figure 2-15 : Processing component | 28 |
| Figure 2-16 : Image processing connection to central data Base..... | 29 |
| Figure 2-17 : User interface for parking application..... | 30 |
| Figure 2-18 : Checking magnetic field parameters | 31 |
| Figure 3-1: System deployment at University of Maryland XX1 parking lot..... | 32 |
| Figure 3-2: Processing results on UMD's XX1 parking lot for seven spots in different days | 33 |
| Figure 3-3: Real-time status of monitored parking spots..... | 34 |
| Figure 4-1 : Step by step research method..... | 35 |
| Figure 4-2 : X-Y values for two different sensors after 360 degree rotation..... | 38 |
| Figure 4-3 : Consistency of calibration results for different sensors in different locations..... | 41 |
| Figure 4-4 : Experiment setup for deriving signature map of the vehicle using array of sensors | 42 |
| Figure 4-5 : Signature of magnetic field amplitude resulting from underneath a vehicle and its neighboring spots . | 43 |
| Figure 4-6 : Location and number of sensors to be installed on parking spots..... | 44 |
| Figure 4-7 : Effect of temperature drifts on reading of sensors | 45 |
| Figure 4-8: Experiment results for calculation of temperature sensitivity in different axes..... | 46 |
| Figure 4-9 : Compensation of temperature drifts | 47 |
| Figure 4-10 : Experiment setup to check linearity effect of neighboring spot's magnetic field interference | 48 |
| Table 4-1 : Experiment Results for Linearity of Cross Interference Effects | 49 |
| Figure 4-11 : experiment results showing linearity effects | 50 |
| Figure 4-12 : Flowchart of processing algorithm | 52 |
| Figure 4-13 : A clustering example for two spots monitored by two sensors | 54 |
| Figure 4-14: Logistic function for one spot..... | 55 |
| Figure 4-15 : Validation of algorithm results with ground truth data | 59 |
| Figure 5-1 : Experiment setup on truck parking field | 60 |
| Table 5-1 : Experiment setup details | 61 |

| | |
|--|----|
| Figure 5-2: Deployment of sensors on truck parking field | 62 |
| Figure 5-3: Packet loss ratio for each spot | 63 |
| Figure 5-4 : Number of events detected during experiment..... | 64 |
| Figure 5-5: Occupancy ratio of different spots during experiment | 65 |
| Figure 5 6 : An example for error rate calculation..... | 66 |
| Figure 5-7 : Error Rates for Each spot | 67 |
| Figure 5-8: Ratio of different type of errors for each spot | 68 |
| Figure 5-9: Distribution of events during the day..... | 69 |
| Figure 5-10: Distribution of average occupancy time during the day | 69 |
| Figure 5-11: Distribution of error rates during the day | 70 |

1 Introduction

Addressing issues such as driver fatigue and the safety of commercial vehicle industry, which is the role of federal government, began in 1937 with the constitution of hours-of-service (HOS) rules by the Interstate Commerce Commission. These rules limit the number of hours that truck drivers may drive before a mandatory rest break. Complying with these regulations has created a demand for parking spaces where commercial vehicle drivers can park and rest. Until recently, a balance existed between this demand for truck parking spaces and available parking spaces. However, changes in the trucking industry beginning in the 1980s increased commercial vehicle traffic, disturbing this balance [1] and creating a growing demand for truck parking facilities throughout the nation, especially in densely populated areas.

When truckers are fatigued or reach their allowable driving time and find that truck parking facilities are full, they are forced to choose between continuing to drive or parking illegally on ramps or shoulders, both of which raise serious safety concerns. The Maryland State Highway Administration (SHA) reported 77 fatal crashes involving large trucks and buses on Maryland highways in 2005 according to the SHA Strategic Highway Safety Plan. One of the priority strategies in the safety area is to reduce the need for trucks to park on high-speed highways, improving safety conditions. Therefore, adequacy of rest area parking is one of the critical issues today and is gaining national importance [2, 3].

A study was carried out by the FHWA in 1996 to investigate the adequacy of truck parking facilities. According to this report, more than 90 percent of drivers interviewed stated that there is a shortage of truck parking at public rest areas. This study also shows that 80 percent of rest areas that provided truck parking were full between midnight and early morning. Researchers

used a nationwide description of truck parking spaces and detailed models of trucker demand to address a perceived need for additional commercial vehicle parking space along U.S. Interstate highways [2]. The June 29-30, 1999, Rest Area Forum in Atlanta, Ga., succeeded in gathering key stakeholders. They agreed that increasing police protection, using appropriate landscaping, improving lighting and developing easy methods of reporting crime could improve rest area safety. They also mentioned that driver education about fatigue and information on the availability of public rest areas and private rest stops are needed. Other issues, such as supporting privately-owned truck stops, providing alternative parking sites, improving provision and location of rest areas, improving financial support of parking and eliminating time limits imposed by states on legal commercial vehicle parking, were also included in the recommendations [4].

The NTSB highway special investigation report, “Truck Parking Areas,” acknowledges a lack of parking spaces and information on parking availability and has information on state-enforced parking time restriction. This study states that the global positioning systems technology combined with electronic maps could be used to help drivers locate parking areas. The study mentions that parking time restrictions for public rest areas can result in drivers returning to the roadway without obtaining adequate rest or parking unsafely on shoulders or ramps [5].

Various states have conducted studies to assess truck-parking requirements. Most of these studies were carried out through direct observation, interviews and surveys. The majority of these studies concluded there is scarcity of parking along interstate highways [6,7,8]. The supply-and-demand analysis and models for commercial heavy truck parking can be found in

different references. As a result of these analyses, shortfalls in the supply were estimated [1, 7, 9, 10].

However, the Maryland Department of Transportation found commercial vehicles parked illegally along Interstate routes during the night, even though an adequate supply of rest areas was available [11]. Therefore, they decided to implement a strategy to inform and educate commercial vehicle operators about available legal parking spots. They added signs along the I-95 corridor to identify facilities with nighttime parking. Also, a map displaying both public and private parking locations was published and distributed to the commercial driver community [9]. The results in [12] indicated almost 70 percent of truckers would use up-to-the-minute information about parking areas when planning their next rest. Also, most of them indicated that road signs, mobile phones and radio were their preferred methods of accessing this information, and almost half said they would reserve a parking spot in advance, preferably by mobile phone [12].

A number of studies offered recommendations to improve the situation, including posting advance parking information in real-time using variable road signs upstream of each parking area, making public-private partnership investments, developing and using ITS and web-based solutions, converting weigh stations near parking facilities into additional parking, allowing overnight parking at mall or large retail chain parking lots, and improving communication regarding state truck parking policies [1, 3, 8, 9, 13].

A study in Virginia listed limitations of conventional data collection methods and investigated potential applications of remote sensing to monitor parking spaces at rest areas [14]. The Federal

Motor Carrier Safety Administration (FMCSA) undertook initiatives to deal with truck parking problems [15].

The basic element of any Intelligent Transportation System (ITS)-based parking information solution is vehicle detection. There are various types of sensors used for vehicle detection, summarized in Table 1-1. Each technology has its own advantages and disadvantages. Some sensors must be embedded in the pavement or attached on the surface of the roadway (in-roadway sensors), and some need to be installed further up from the surface of the roadway (over-roadway sensors).

Table 1-1: Types of sensors used for parking application

| in-roadway sensors | over-roadway sensors |
|---------------------------|--|
| inductive loop detectors | video, image, and acoustic signal processors |
| pneumatic road tubes | microwave radar |
| piezoelectric | ultrasonic |
| magnetic sensors | infrared sensors |

An inductive loop detector (ILD) consists of one or more turns of insulated wire buried in in the roadway, a lead-in cable that runs from a roadside pull box to the controller cabinet and an electronics unit located in the controller cabinet. Together they detect the vehicle by means of the electrical signals induced when a vehicle passes over or stops within the loop. The operation of inductive loop sensors is well understood, and their application for providing basic traffic parameters (volume, presence, occupancy, speed, headway, and gap) represents a mature

technology. The equipment cost of inductive loop sensors is low when compared to over-roadway sensors.

Inductive loop detectors, however, are among the most intrusive technologies; they require cutting the pavement and installing extensive wiring. In many instances, multiple detectors are required to instrument a location. Additionally, roadway resurfacing and utility repair creates the need to reinstall these types of sensors. The wire loops are also subject to the stresses of traffic and temperature. Therefore, installation and maintenance costs significantly increase the life-cycle cost of inductive loop detectors.

Pneumatic road tubes work by sending a burst of air pressure along a rubber tube when a vehicle's tires pass over the tube. The pressure pulse closes an air switch, producing an electrical signal that is transmitted to a counter or analysis software. Advantages of road tube sensors include quick installation for temporary recording of data and low power usage. Disadvantages include inaccurate axle counting, temperature sensitivity of the air switch and cut tubes from vandalism and truck tire wear.

Piezoelectric sensors are composed of a coaxial cable with piezoelectric materials surrounding a solid copper core placed in the middle of another solid copper casing and generating an electrostatic charge proportional to the input force resulted from the weight of the vehicle. These sensors are well suited to weigh-in-motion measurements. When properly installed and calibrated, these sensors and their associated electronic logic can weigh all types of vehicles moving at various speeds. However, they are very expensive and subject to some of the same problems as the vehicle inductive loop sensors. To maximize their accuracy, these systems require a considerable amount of calibration.

Video image processor systems detect vehicles by analyzing the imagery from a traffic scene to determine changes between successive frames. Image processing continually improves in its ability to compensate shadows, reflections, camera motion, etc. However, like most of the over-roadway technologies, these systems generally consume a large amount of power, demand large communication bandwidth, are weather-sensitive and are expensive to deploy and maintain.

Microwave radar sensors transmit energy toward an area of the roadway from an overhead antenna. The area in which the radar energy is transmitted is controlled by the size of the antenna coverage area and the distribution of energy across the aperture of the antenna. Unlike video image processors, microwave radars are less sensitive to environmental conditions; however, they are ineffective at detecting stopped vehicles.

Ultrasonic sensors transmit pressure waves of sound energy at frequencies above the human audible range to recognize vehicles. They measure distances to the road surface and vehicle surface by detecting the portion of the transmitted energy reflected towards the sensor from an area defined by the transmitter's beam width. They are very easy to install; however, they are sensitive to temperature changes and air turbulences.

Two types of infrared sensors, active and passive sensors, may also be used.. Active infrared sensors use laser diodes to illuminate the detection area with infrared wavelength light and detect the reflection transmitted by the vehicle. Passive sensors do not illuminate but instead detect the emitted infrared energy from the vehicle. Their installation is relatively easy (especially for passive infrared sensors) and by using multiple illuminator laser diodes for active infrared sensors, vehicle speed, length and position can be measured. Interference of other sources of

infrared emission, atmospheric particles and weather conditions such as fog, rain and snow all affect the performance of infrared sensors.

Relative average purchase cost of different types of sensors can be compared in Figure 1-1. In this chart, the cost of technology gets higher as one moves further from the center, so magnetic sensors are less costly relative to the competitive technologies.

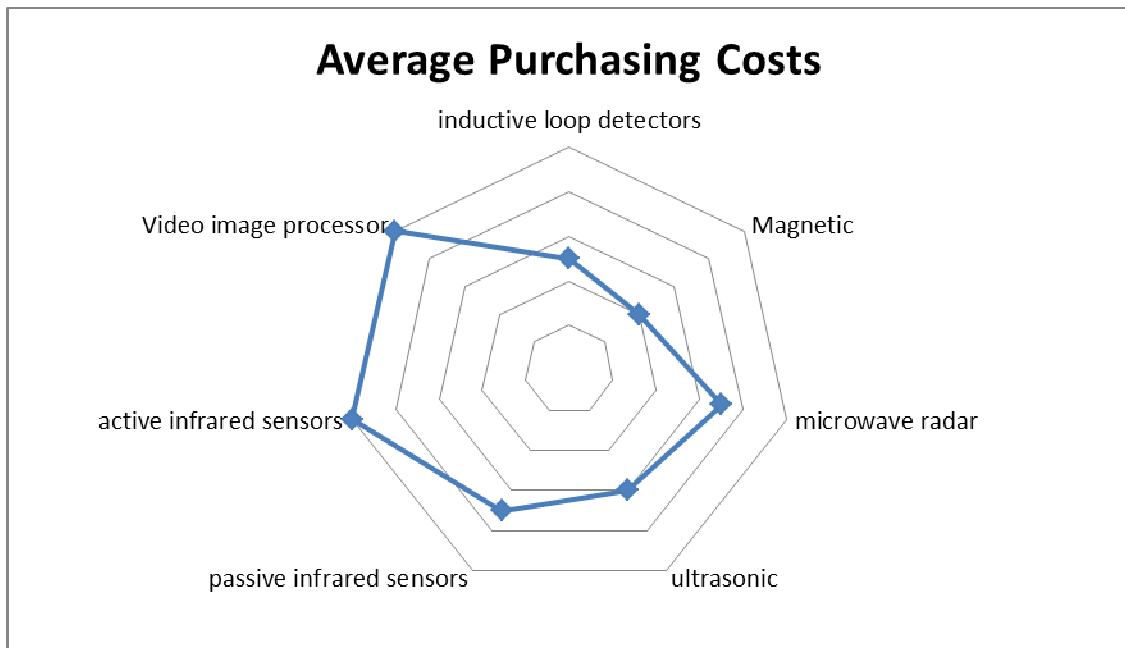


Figure 1-1: Relative cost comparison for different types of sensors

Motivated by the use of technology to improve truck parking safety through efficient use of existing parking capacity, this project aims to develop an automated real-time parking information system by employing low power wireless vehicle detection technology. By using this new technology, the parking monitoring system is low-cost, scalable, layout-independent and easy to deploy. Unlike image-based technologies, the system is completely anonymous and thus the privacy of truckers is not compromised. Wireless detectors used in this project are a

modified version of sensors previously developed through a project sponsored by the Maryland State Highway Administration [16].

The main goal of this project was to develop an inexpensive and scalable wireless sensor network prototype, which encompasses a cost-effective and reliable architecture for detection of trucks and other vehicles in parking lots. The wireless sensors are equipped with the necessary instrumentation components, such as Anisotropic Magneto-resistance elements for the purpose of detecting trucks. These sensors communicate to a local base station by means of short-range radio transmissions and form a wireless mesh network. The local station is connected to a remote server and forwards the collected raw measurements for further processing and identification of the status of the spots. The sensors are power-efficient and use IEEE 802.15.4 standard for local communication - the most power-efficient standard for short-range wireless applications. Figure 1-2 shows a simplified schematic of the architecture developed for this solution.

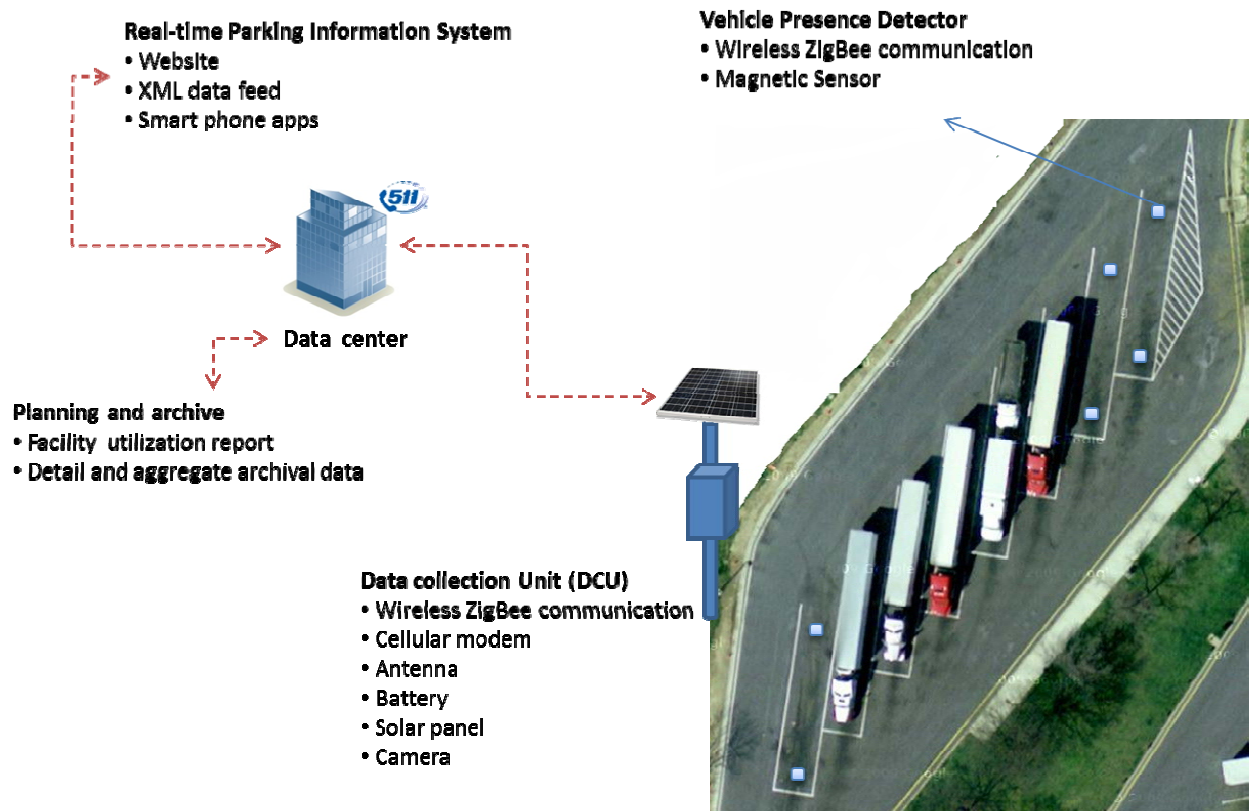


Figure 1-2: Schematic of parking information system design

As Figure 1-2 shows, sensors are deployed on the parking spots and a remote sensor can communicate with local station connected to the remote location by means of cellular broadband communication. The range of short-range wireless networks is limited to 100 meters (328ft) based on the regulations set for maximum allowable transmission power of devices. However, multiple local stations can be deployed if the size of parking lot is too large to be covered by just one station.

the data through TCP/IP protocols, parses the data, extracts the information and transfers the information to databases. A processing component then processes the updated information inserted to the database and updates the status of the spots in the parking lot. The UI component consists of developed software that remotely connects to the servers and checks the status of the spots, along with other necessary information for administrators to control the performance of the system. In this section, each of these four components, which are the building blocks of the parking monitoring solution, will be explained in detail.

2.1 Sensing Component

The sensing component performs three main tasks: sensing, wrapping the raw data into packets and transmitting the packets of data to the local stations. The architecture of the sensing component includes the following elements: Sensor, Power Supply, RF Antenna and Microcontroller, as illustrated in Figure 2-2.

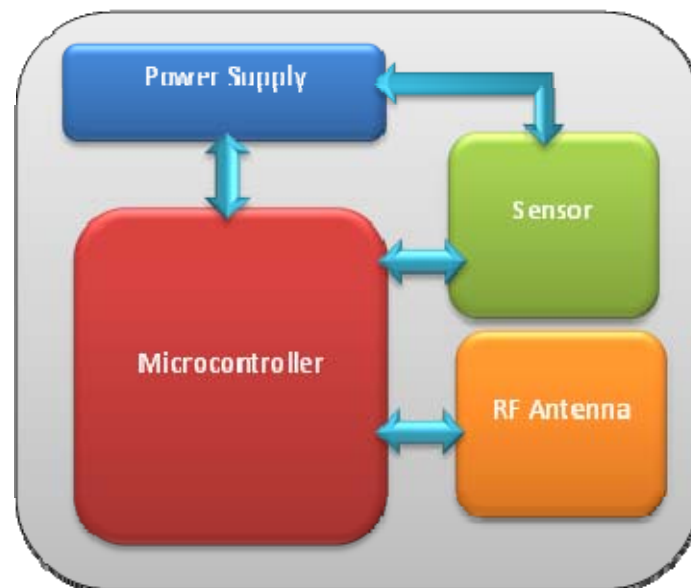


Figure 2-2: Sensing component

2.1.1 Sensor

In order to detect vehicles, magnetic sensors were embedded in the sensing component. A magnetic sensor generates a digital signature of a passing vehicle based on disturbance of the magnetic field caused by ferromagnetic material of the vehicle. When a vehicle passes the proximity of a sensor, the large mass of steel and other ferromagnetic material in the vehicle's body causes a strong disturbance and the magnetic signature of the vehicle can be measured. The signature is collected in three dimensions, each of which has a wave form. There are two types of sensors that can be used for vehicle detection using magnetic field measurement: Anisotropic Magneto-Resistive (AMR) and Giant Magneto-Resistive (GMR). AMR sensors are directional sensors and can provide only an amplitude response to magnetic fields in their sensitive axis.

Based on the previous experience of the research team in the "Traffic Data Collection and Anonymous Vehicle Detection Using Wireless Sensor Networks" project conducted for Maryland State Highway Administration (SHA), AMR sensors were selected for this project. Compared to GMR sensors, AMR sensors are more sensitive to the change in the magnetic field. Even very small magnetic fluctuations can be tracked effectively by using AMR sensors. In the processing of the data, which will be discussed later, it is important to have a uniform measurement of different magnetic sensors installed on different spots. If the magnetic response is not linear, the measurements would be complex and less effective.

Although the solution works for any parking facility, in this project the system is customized for a truck parking application. One issue in detection of trucks is their chassis' high distance from the ground compared to passenger cars. Since sensors are installed on the ground, higher clearance means less variation in magnetic field when a truck approaches the sensing area. To

address this issue, the system’s sensitivity to the magnetic field was calibrated and optimized compared to the traffic measurement sensors used in the Inter-County Connector deployment. However, increasing the sensitivity of sensors has a major drawback: the increase of temperature drifts and temperature noise power density.

The AMR sensors consist of magneto-resistive elements oriented on a “wheatstone bridge.” The resistances of such elements change when exposed to a magnetic field. By selecting higher gains for the magnetic sensors to be more sensitive, the resistance of magneto-resistive elements will decrease, making them more sensitive to temperature variations. If the resistance of the magneto-resistive elements changes by the temperature, reading of the sensor (which directly corresponds to the resistance of the resistors) varies without a change in the magnetic field. As Figure 2-3 illustrates, the sensors show more vulnerability in regard to temperature noise.

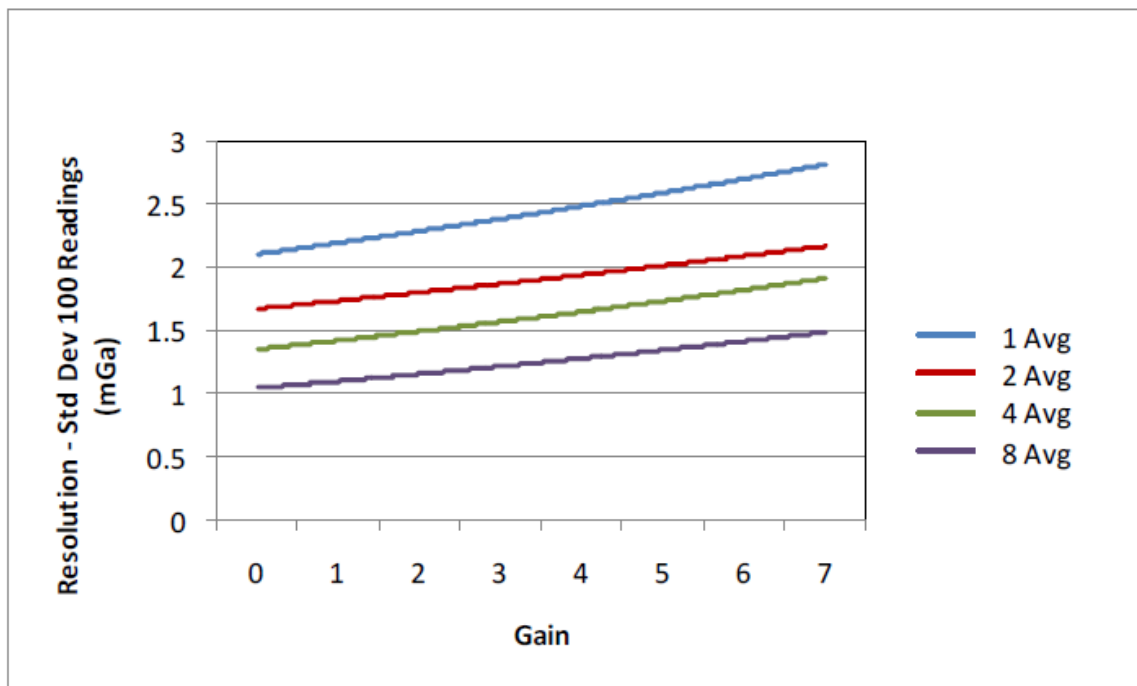


Figure 2-3: Sensitivity of Magnetic Sensors

To address the issue of high chassis distance from the sensors, sensitivity of the sensors increased to ± 0.88 Gauss; concurrently, software solutions were developed to compensate the temperature vulnerability caused by this sensitivity increase. The temperature compensation methods are discussed later in the report.

2.1.2 Power Supply

Collecting data via the sensors, processing data and transmitting the bundled packets of data consume power, and since the system should be designed for minimum human maintenance, a reliable power source needs to be utilized along with optimized power consumption. To find the required power supply for the sensing component, a number of experiments were designed and conducted by the research team.

The performance of short-range wireless systems is limited to the environmental effects such as interference effects, shadowing, multipath fading and temperature noise. With these inevitable sources of signal degradation, packet loss, which leads to the loss of information, is observed in any system. One solution to this issue is to increase the sample rate or duplicate data and transmit the same data several times. However, increasing the sample rate will cause higher power consumption.

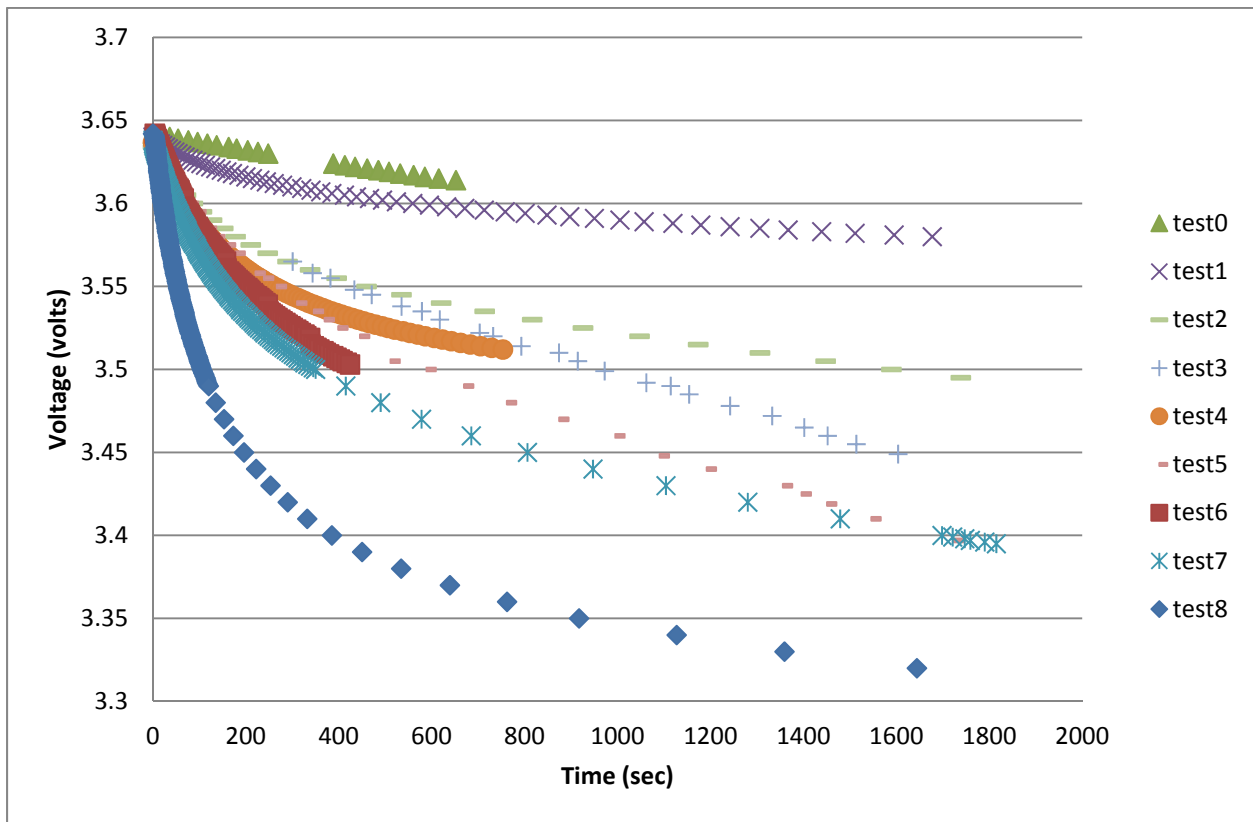
The research team conducted power consumption experiments; firstly, the relationship between the sampling rate and power consumption was examined, and then the inefficiencies of hardware manufacturing and assembly were tested. There are two sources of power consumption in the sensing component:

- Transmission

- Data collection

Experiments were designed to test each type of consumption separately. Regarding the operating DC voltage range for the microcontroller, which is 2 volts to 3.6 volts, a super capacitor with 0.4F capacitance was charged to the maximum level of the voltage range and then connected to the sensing component to supply it with the required power. The voltage of the capacity was carefully monitored to derive the curve of power consumption over time. Since the relationship between the current and the voltage of the capacitor is $i_c = C \frac{dV_c}{dt}$, we can measure the power consumption of the system as $p = CV_c \frac{dV_c}{dt}$. Hence, a separate test was conducted for each of the mentioned types of the power consumption.

As Figure 2-4 shows, increasing the sampling rate increases the power consumption, which is observed in a higher rate of voltage drop of the capacitor. Figure 2-4 also shows that transmission of the packets over the air increases the power consumption compared to the case where the only source of power consumption is the sensor and its data collection.



| | Test0 | Test1 | Test2 | Test3 | Test4 | Test5 | Test6 | Test7 | Test8 |
|-----------------|-------|--------|-------|-------|--------|-------|-------|-------|--------|
| Data Collection | × | ✓ | ✓ | ✓ | ✓ | ✓ | ✓ | ✓ | ✓ |
| Transmission | × | × | × | × | × | ✓ | ✓ | ✓ | ✓ |
| Sampling Period | × | 10 sec | 5 sec | 1 sec | 0.1sec | 10sec | 5sec | 1sec | 0.1sec |

Figure 2-4 : Experiment results for power consumption

Based on the experiment results and using the power consumption formula ($p = CV_c \frac{dV_c}{dt}$), and assuming 3.4 watt hours batteries, the lifetime of the sensing component for each of the tested sampling periods are shown on the left side of Figure 2-5. The right side of Figure 2-5 shows instrument setup for such measurements.

| Sampling Period | Time limit(Day) |
|-----------------|-----------------|
| 0.1sec | 23.36 |
| 1 sec | 217.36 |
| 5 sec | 729.05 |
| 10 sec | 1631.24 |

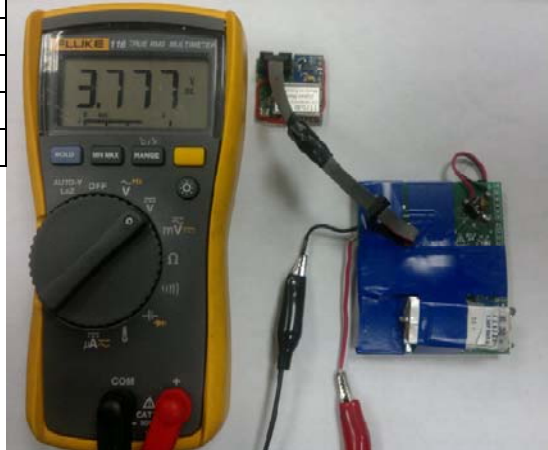


Figure 2-5: Setup to measure power consumption

Unlike the highway application in which solar panels were used to power up the sensors, relying on solar energy in this project was not possible. Due to extended parking sessions, sensors did not have access to sunlight for the majority of their operation time. Power consumption of the sensing component is related to the sampling rate of the sensors, which determines the frequency of samplings and transmission. On the other hand, sampling rate should be carefully selected regarding the dynamicity of the parking lot. In this project, two AA 1.5 volts batteries were used in series to supply the sensing component with the required power.

2.1.3 RF Antenna

This component includes a communication antenna and the necessary circuits for wakeup scheduling, instrumentation, amplification and communication. Due to path loss, shadowing and

multipath fading, the quality of the link between the sensing component and the collecting component deteriorates. The physical range in ZigBee protocol is approximately 10-100 meters (33-328 ft); however, environmental obstacles such as buildings, trees and vehicles may seriously weaken the signal and lead to packet loss. Link Quality Indication (LQI) is a quality indicator provided by ZigBee protocol and can be used to improve the localization in a wireless sensor network. Analysis of LQI helps select the best RF antenna type for the sensors and also helps determine the best direction for sensors and collector antennas to achieve highest directivity. Low LQI results in packet loss, which is a major problem for vehicle detection. An experiment was designed using three different sensors to find the largest possible distance between sensors and the collector that ensures communication link quality.

As shown in Figure 2-6, three sensors were installed in four different distances (10, 20, 30 and 50 meters) from the collector. The LQI and packet loss was measured repeatedly for each sensor in different settings. Results, illustrated in Figure 2-7, show that increase in distance between sensors and collector from 30 meters to 50 meters considerably decreases the LQI for all three sensors and leads to an almost 100 percent increase in packet loss ratio. Packet loss ratio is a measure showing the percentage of packets sent by the sensors that cannot be received at the collector. This decrease in LQI is due to path loss or path attenuation, a physical attribute of electromagnetic waves.

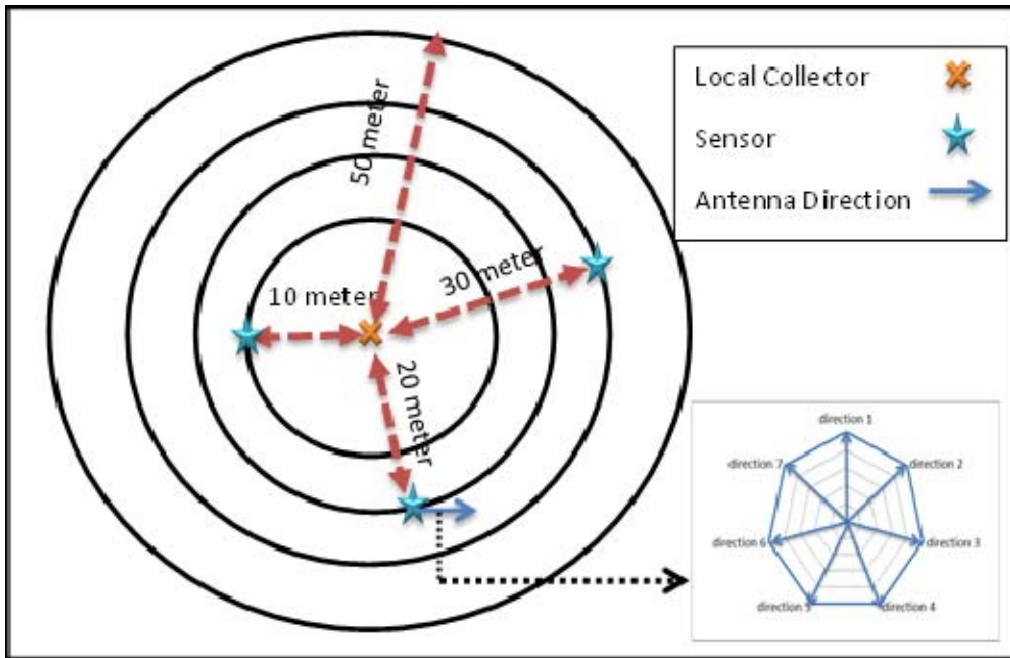


Figure 2-6: Experiment setup for testing link quality and packet loss

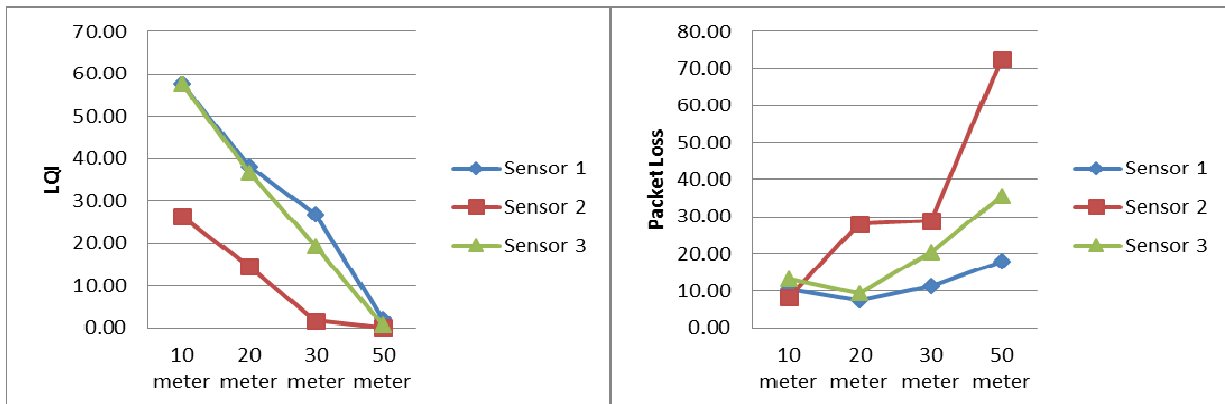


Figure 2-7: Results of LQI and packet loss experiments

In addition to the sensor-collector distance, direction of RF antenna is also an important factor that affects the quality of the radio link. As demonstrated in Figure 2-6, direction of sensors' antenna was rotated 360 degrees and the LQI of the signals and packet loss for each direction

were measured in different distances. Figure 2-8 shows that LQI is directly affected by the direction of the antenna; thus, antenna direction must be carefully chosen to minimize the loss.

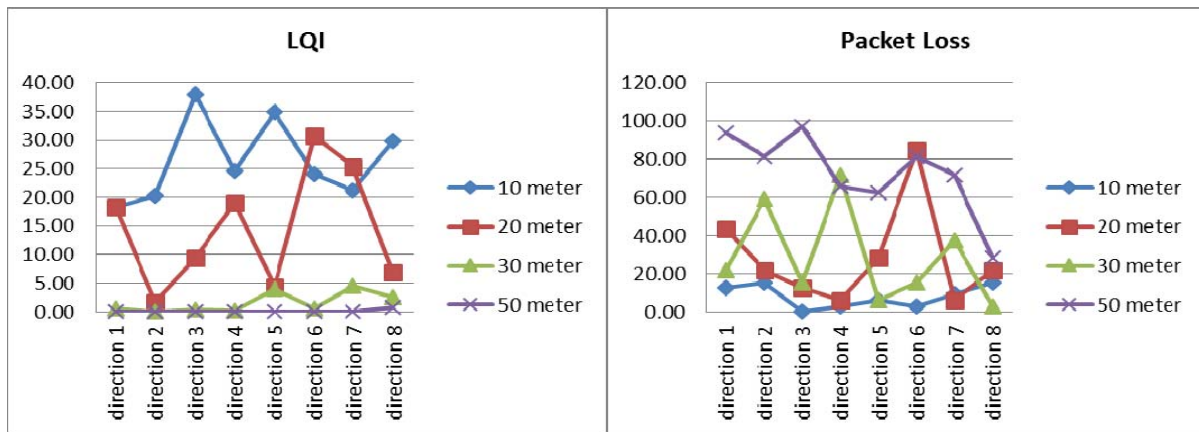


Figure 2-8: Directional tests on connectivity performance

For this project, two types of antennas were tested and used: monopole antennas and patch antennas. The patch antenna's directivity is higher than monopole antenna's and can support higher gain and consequently higher LQI when there is a line of sight between the transmitter and the receiver. However, monopole antenna is less risky in environments with obstacles such as buildings and trees. Because most trucks have high clearance from the ground and other obstacles are not present on the parking site, both transmitters and receivers have a fair enough chance of having line of site; thus, both antenna types can be used. Figure 2-9 shows both antenna types.



Figure 2-9: Antenna types

2.1.4 Microcontroller

This component controls and implements all the sensing and wireless communication operations required based on the embedded programs developed by the project team exclusively for this solution. For the purpose of this project, based on the successful experience gained from the former “Traffic Data Collection Project” [16], TI’s CC2530 was selected to support wireless communication for the sensing component. TI’s CC2530 is both fast and energy efficient enough to handle magnetic sensors. This sensor is a System-on-Chip (SoC) solution, which combines the industry-leading radio 2.4 GHz transceiver of the IEEE 802.15.4 with an industry proven, compact and efficient 8051 microcontroller. The CC2530 also provides a relatively large flash memory size of up to 256 KB, which makes it suitable for ZigBee PRO applications.

2.1.5 Enclosure Design

Deployment of sensors for parking application requires careful consideration for designing an appropriate enclosure that can both protect the electronic devices against harsh environmental conditions such as rain and humidity and tolerate the weight of vehicles. It must also promise reliable radio link connectivity. Several prototypes were designed and tested for this purpose,

and based on experiments, necessary modifications were applied. For protection against humidity and temperature changes, a waterproof sealant was applied to the circuits and devices. A product from TAP Plastics called EasyCast was used for this purpose.

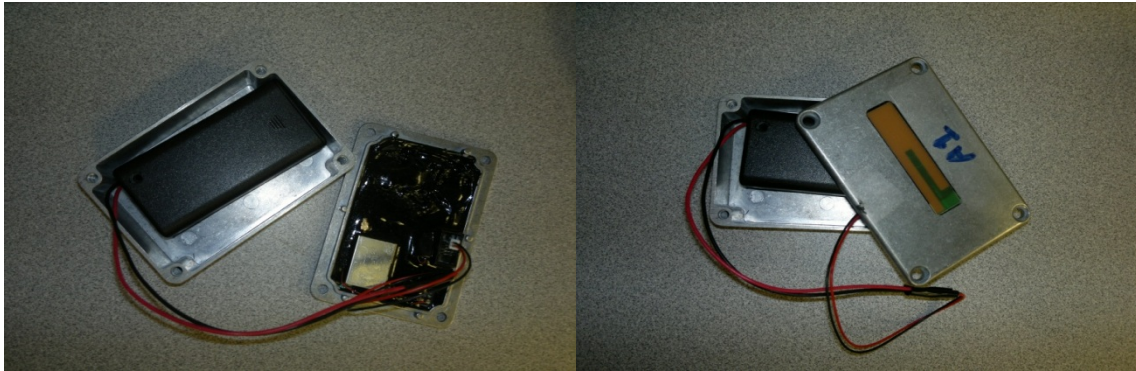


Figure 2-10 Enclosure Design

After conducting extensive research on the candidate materials and to make the custom-designed enclosure, the research team decided to use an encasement attached to the electronic board that is casted on the cap of the encasement. The antenna was mounted on the cap. Patch antennas were incorporated into the final device. In addition to its advantages of directivity and RF antenna gain, its flat design allows easy installation on the surface of the case. As shown in Figure 2-10 the empty space inside the encasement is used for adding AA batteries that can promise several years of power supply for the sensor.

2.2 Collecting Component

One of the main components of the traffic detection system is the local station, which collects data from the deployed sensors on the nearby parking lot spots. This component also acts as a gateway between the Zigbee-based network and the IP network over which the data is carried. The architecture of the collecting component includes following elements: Microcontroller, Power Supply, RF Antenna and Cellular Broadband Transceiver. For the purpose of testing the

system performance and providing ground truth data, a camera was also added to the system. The camera is necessary for testing and validation and is not an essential component of the final truck parking information system. Figure 2-11 shows a block diagram of the system.

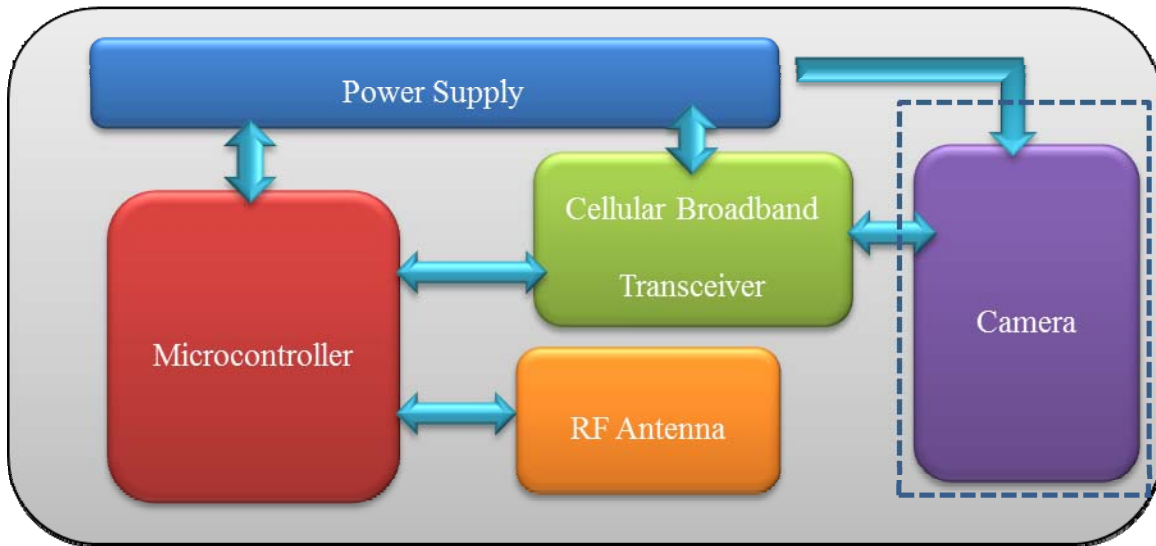


Figure 2-11 Block diagram of data collector

2.2.1 Microcontroller

The same TICC2530 microcontroller used in sensors was selected for the data collector. Modifications in the embedded code were implemented to accommodate the following functionalities: data collection and packaging, link quality measurement and reporting, voltage levels, and continuous health monitoring of the deployed components.

2.2.2 RF Antenna

For the local station, a monopole antenna was selected to reliably capture the electromagnetic waves from sensors deployed in different locations. If a highly directional antenna is used, there might be little chance to have enough link quality for all the sensors in the network. By

employing a monopole antenna with a distributed gain pattern, it is more likely to have a fair link quality for all sensors. This is especially true if at the sensor side, a high gain antenna with enough directionality is deployed.

2.2.3 Cellular Broadband Transceiver

A cellular broadband system was designed and installed on the collecting component to connect the embedded system to the IP network for further processing of collected data at the remote station. One of the best solutions was using a cellular modem (such as CDMA or GPRS modems offered by telecom carriers), which is connected to the microcontroller. The modem receives the raw packets from sensors based on commands issued by the microcontroller, and it forwards the data to the IP address of the remote station. Using cellular modems is the most power- and cost-efficient solution when the system is finalized and has passed all performance tests.

To accommodate simultaneous data and video collection in this project, a Linux-based system was designed to reliably and remotely control the performance of the vehicle detection system. The system reads data to the microcontroller through its serial port and concurrently connects to the AT&T cellular network. At the same time, it controls image capture to provide ground truth information. This system enables the remote station to be able to access and fully control components of the local station such as the camera and microcontroller at any time. The operation flow of this system is depicted in Figure 2-12.

As Figure 2-12 shows, the Cellular Broadband Transceiver (CBT) works as a gateway between the remote station (RS) and main elements of local station, including the microcontroller and the camera. CBT gets initialized by the RS through the cellular network and updates the RS by providing necessary information such as network status, timings and access information. RS sets

both the sampling rates of the camera and the rates for the data transmission from the CBT to the RS. Consequently, RS sends commands to the CBT to enable the microcontroller to start data collection; CBT enables the microcontroller to start writing the data on the serial port and immediately informs the RS that data collection has been started. As soon as the RS receives data collection acknowledgement from the CBT, it sends commands to CBT to enable the camera. At any time, RS can disable both data collection and the camera or re-enable them..

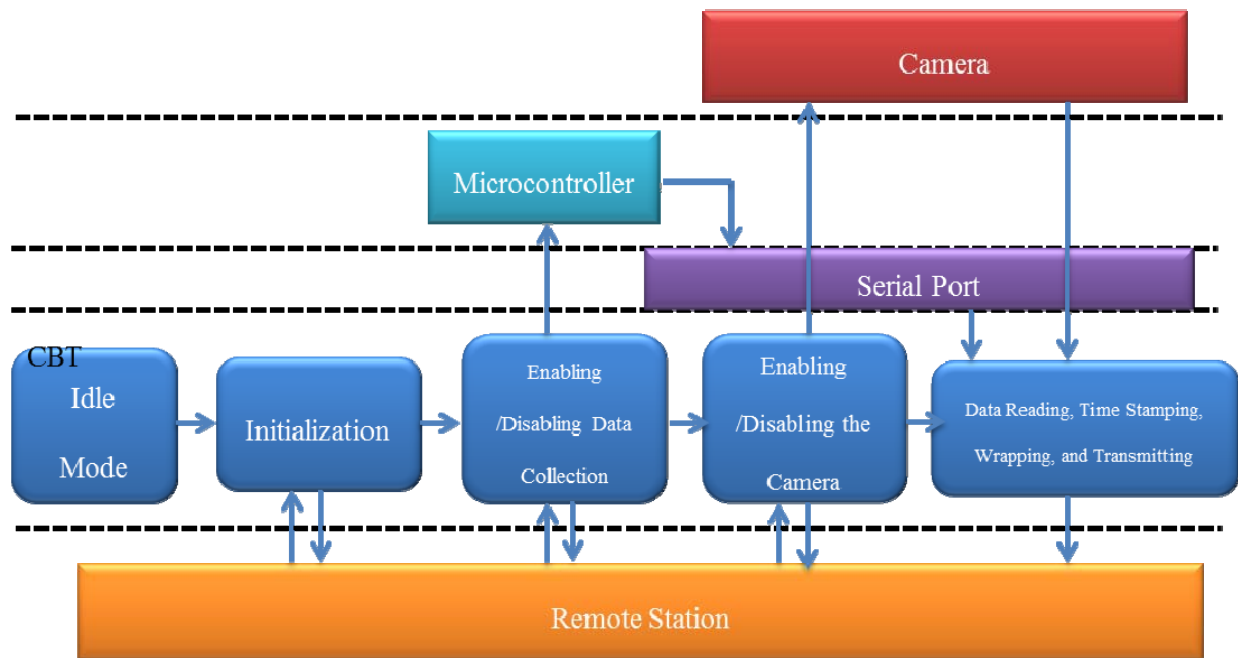


Figure 2-12 : Operational flow for cellular broadband transceiver (CBT)

After enabling the microcontroller and data collection based on the settings done in the initialization period, CBT receives both ZigBee packets and images periodically, adding time stamps on them that are crucial for processing. During each file transmission period (also set in initialization), CBT wraps all the data and images in a zip file and transmits it to the remote

station and waits until the next period to repeat the operations or to receive a command from the RS. This system was proven to be very reliable during the experiment and had been operating without any disruption for three months.

2.2.4 Camera

A camera is added to the local station for testing and validation purposes and is not necessary in the final solution. The period for capturing images from the parking spots should be set in regard to dynamicity of the parking lot. During busy hours where parking lots experience the highest dynamicity, one-minute intervals can provide solid ground truth. However, the interval is not fixed and the sampling rate for the camera can be updated and modified during different times of the day or under special circumstances. The CBT adds a time tag on the images to be used for processing. Figure 2-13 shows a sample still shot from the camera.



Figure 2-13 : Image sample captured and time stamped by the collecting component

2.2.5 Power Supply

The local station needs considerably more power since it should connect to the cellular network to transmit and receive data. For the purpose of validation, cellular broadband transceiver's functionalities were enhanced in this project and a camera was added to the system, increasing power consumption. Figure 2-14 shows verification of power supply system.

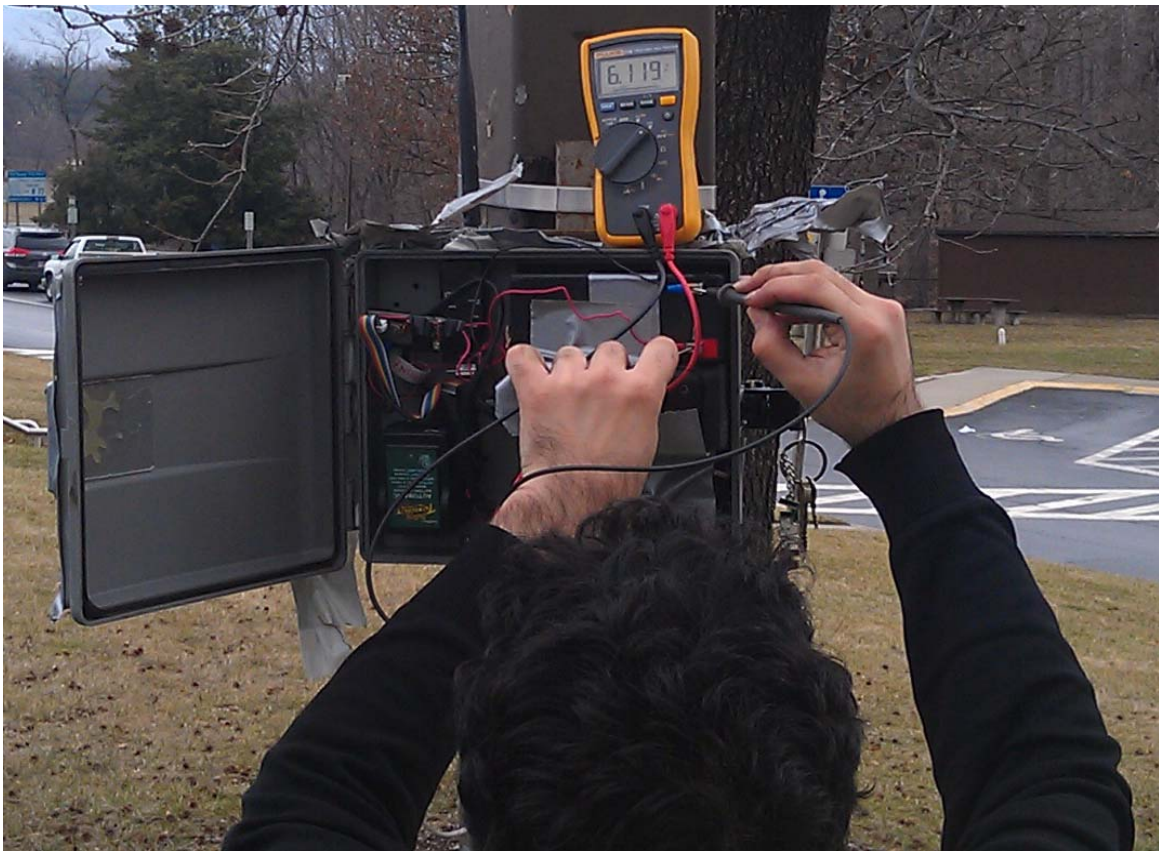


Figure 2-14 : Power supply sub-system of the collecting component

To empower the local station for the required power, a rechargeable lead-acid battery with 12 volts and 9Ah specifications was initially used, which lasted 48 hours. To increase the experiment time, a request for access to available power lines was sent to SHA on Sept. 7, 2012. Due to some technical issues raised by the related facility managers, the power outlets could not

be accessed until January 2013. Once the outlet was ready, a transformer was used to charge the rechargeable batteries every night and continuous performance of the system was possible.

2.3 Processing Component

The processing component is responsible for receiving data from the local stations, organizing the data and processing it to determine the status of each monitored spot of the parking lot. It consists of four major components: TCP/IP Listener, Central Database, Image Processor and Data processor, as shown in Figure 2-15.

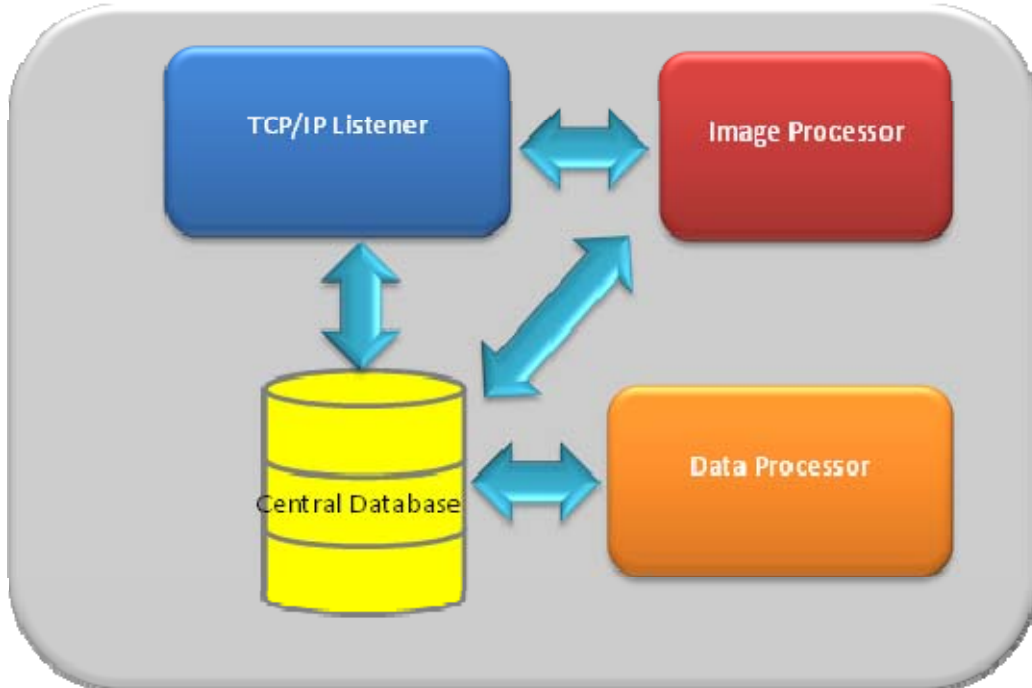


Figure 2-15 : Processing component

TCP/IP listener waits for the incoming stream of data and images through IP networks. Once it receives a package, it unwraps the data and extracts signals collected by sensors and images captured by the camera. TCP/IP listener parses the collected data and inserts them into a central

database. It also organizes the received images and transfers them to the Image Processor components for extracting the ground truth results.

The central database is designed and implemented to save all the raw data collected by the local stations, provide the processing component with necessary data, save the results of the processing algorithms, and provide clients who request access to the database with the updated status of spots.

The Image Processor component, which searches for any change in the status of the spots and in case of any change, connects to the central database and inserts information about that change to be saved and processed later. This way, performance of algorithms designed to process the collected data of magnetic sensors can be validated. As illustrated in Figure 2-16, a tool was developed to support image processing by importing the events (Arriving or Leaving of a Vehicle), their associated time and other information such as vehicle type and direction of parking (head- in or tail-in) to the database.

The screenshot shows a Windows application window titled "Form1". It contains a date calendar for March 2013 with the 1st selected. Below the calendar are time selection dropdowns for hh (11), mm (53), and ss (24). There are three dropdown menus for "Event Type" (Left), "Type of Vehicle" (SUV), and "Direction" (Head_in). A text input field for "spotNumber" contains the value "4". There is also an "Other" text input field. On the right side, there are several dropdown menus: "SERVER" (129.2.133.1), "PORT" (3306), "USERNAME" (root), "PASSWORD" (masked with asterisks), "DATABASE" (Parking), and "Table" (Events). Below these are three buttons: "Connect", "Refresh", and "Add".

Figure 2-16 : Image processing connection to central data Base

Data processing component checks the central database for any updates of the received raw data from the sensors and processes them with decision-making algorithms to decide whether status of a particular spot has changed. After processing, this component updates the central database with the latest status of the spots.

2.4 User Interface Component

To observe the solution results, a User Interface (UI) is required for the clients to access the central database of the processing component and check for the last update of the system. Figure 2-17 shows a TCP/IP UI designed for this project. This interface supports functionalities such as Log In, Load Data, Process Data, Ground Truth, Visualization, Output Selection and Calibration.

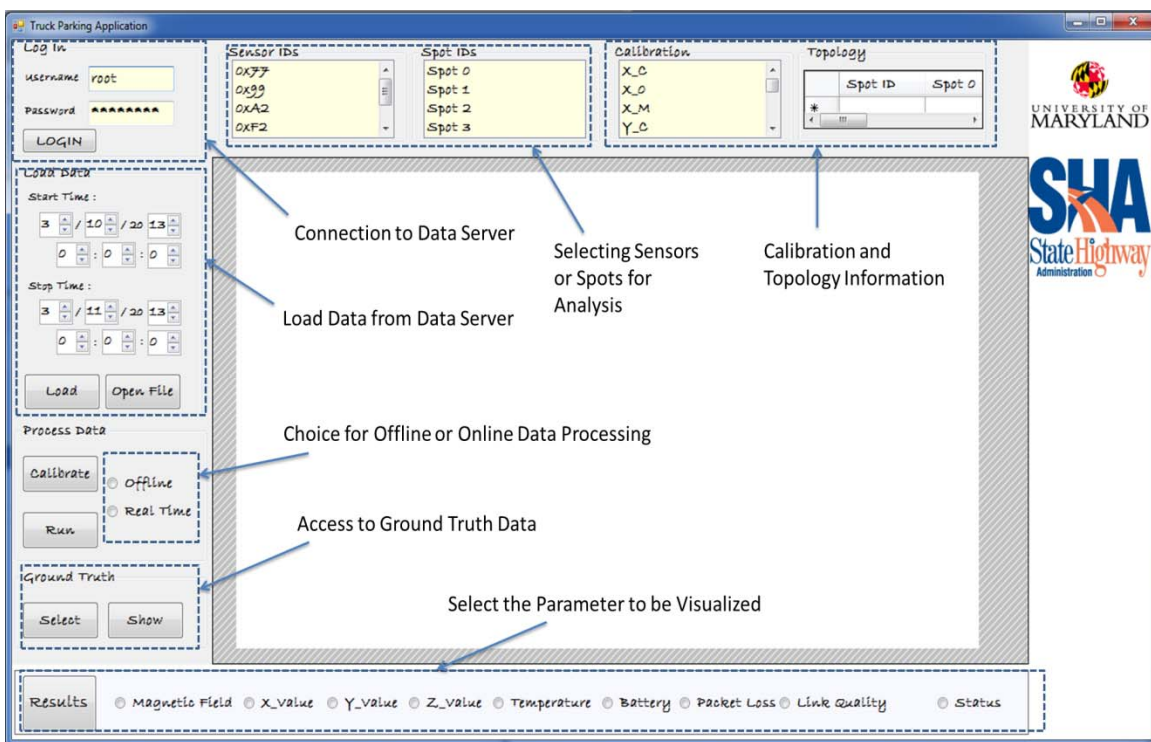


Figure 2-17 : User interface for parking application

For each user, a username and password is necessary to access the database. After successful login, a user can choose to access the real-time data in the database to check the status of each spot or can access the archived and analyzed historical data. For offline access, a user should provide start-time and stop-time to select data corresponding to the selected interval. Then the user can run data processing within the selected time interval to obtain information per spots or sensors.

On the administrator side, it is important to always monitor important indexes such as magnetic field detected by the sensors, link quality index, voltage of the box, etc. The user interface is designed to monitor such metrics. For example, as illustrated in Figure 2-18, the magnetic fields of three different spots measured by three sensors are plotted within a one-hour period selected by the user.

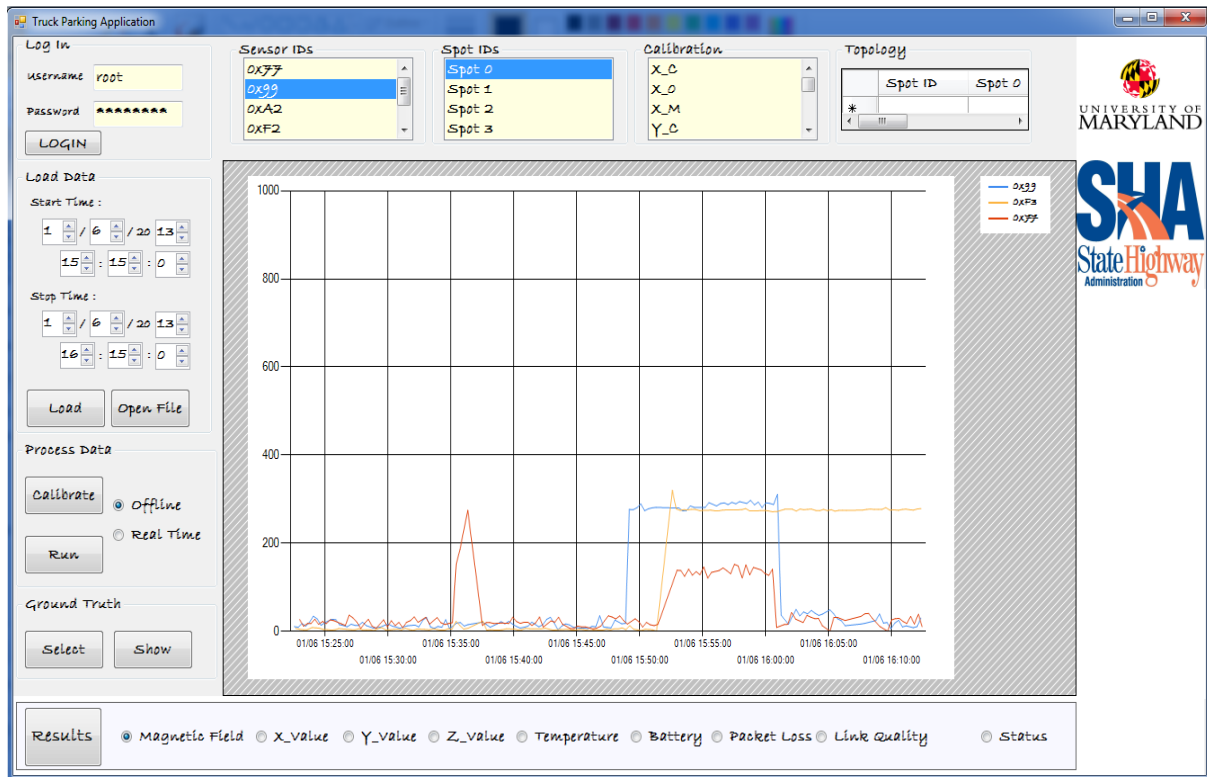


Figure 2-18 : Checking magnetic field parameters

3 System Deployment on UMD Campus

To prepare for the actual deployment, multiple experiments were conducted on UMD campus parking lots. As illustrated in Figure 3-1, a local collector powered by a solar panel was used to monitor seven parking spots at UMD's XX1 parking lot.



Figure 3-1: System deployment at University of Maryland XX1 parking lot

The extensive preliminary data collection at this experimental deployment helped explore possible issues such as temperature drifts, cross-magnetic interferences and packet loss. Results were analyzed to find solutions for different possible scenarios and develop the initial processing algorithms. Developing algorithms for decision-making about the presence of vehicles on spots requires a supervised learning time to find the best clustering on the collected data. A camera

was incorporated into the data collector box to collect ground-truth imagery during the experiments. As illustrated in Figure 3-2, collected data were processed for different days on seven spots. An initial decision making algorithm was designed, implemented and calibrated.

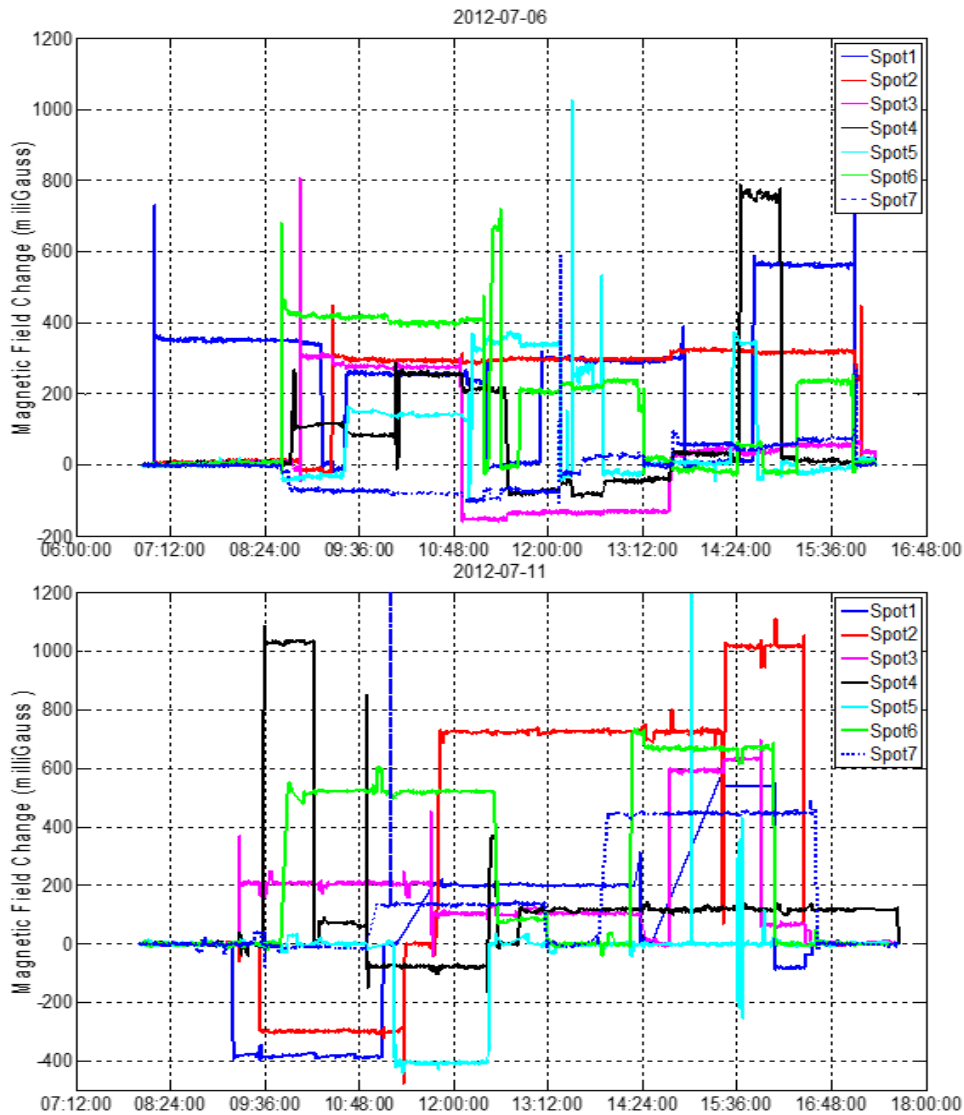


Figure 3-2: Processing results on UMD's XXI parking lot for seven spots in different days

During the tests, real-time monitoring of the parking spots was conducted, and necessary modifications for each of the four major components of the solution were implemented. A demo

was also presented to UMD's Transportation Services in return for their permission and cooperation for deployment of the system on campus premises. Figure 3-3 shows snapshots of the system during such experiments.

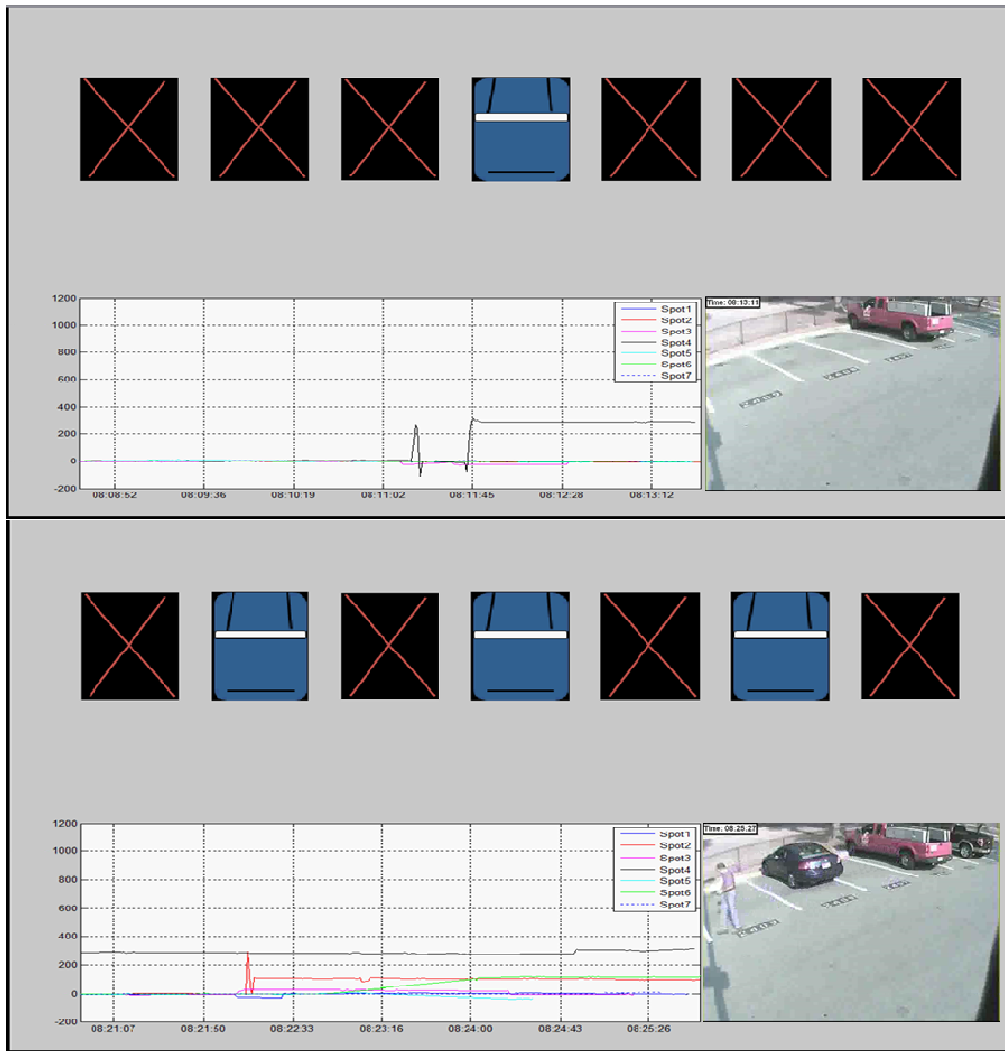


Figure 3-3: Real-time status of monitored parking spots

Several rounds of additional experiments such as packet loss tests, antenna direction tests and enclosure design tests were also conducted during this deployment prior to deploying the system in the rest area truck parking facility.

4 Signal Processing and Results

To develop the processing algorithms for decision-making on the presence of vehicles in parking spots, a five-step approach depicted in Figure 4-1 was developed. First, data collected by magnetic sensors were analyzed and interpreted to meaningful parameters, and a calibration method was developed to give uniform results while testing different sensors in similar circumstances. The next step was to analyze the magnetic effect of vehicles. By testing different types of vehicles, the research team statistically detected a trend for the magnitude of magnetic distribution in different positions underneath the vehicles.

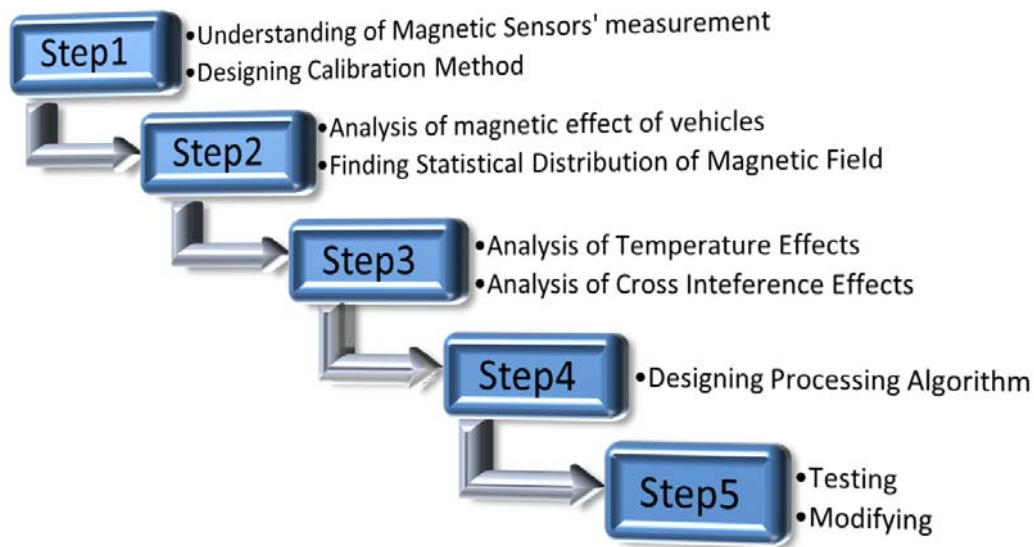


Figure 4-1 : Step by step research method

During field experiments, it was noticed that temperature change has direct and considerable effects on the measurement results of magnetic sensors. A number of experiments were hence conducted to find a relationship between measurements and temperature. The behavior of interfering cross effects of vehicles parked in neighboring spots on the magnetic field sensed by

sensors was also measured, since it could impose considerable effects on processing and decision-making. Based on the findings in the previous steps, an algorithm was designed and developed to detect vehicles using the processed data collected by network of sensors. The algorithm was revised and optimized based on the experiment results to enhance the robustness and accuracy. For validation and quality control, ground-truth data generated through images captured every minute were used to check the status of parking spots and compare it with results of the processing algorithm. This section describes each step in detail.

4.1 Magnetic Sensors' Output Data and Calibration

Magnetic sensors measure the gradient of magnetic field's magnitude. The sensors consist of resistors sensitive to a magnetic field, and they measure magnetic field elements in three vertical axes. However, it is almost impossible to have ideal resistors with 100 percent identical offset and sensitivity to the magnetic field. If two different sensors of the same type are used in exactly the same direction and at the same point, values for the X-axis, Y-axis and Z-axis will not necessarily be equal. Adding the sensor to the electronic board, casting the board and installing the casted board in metal cases are other ways to have different offsets in each of three dimensions for different sensors.

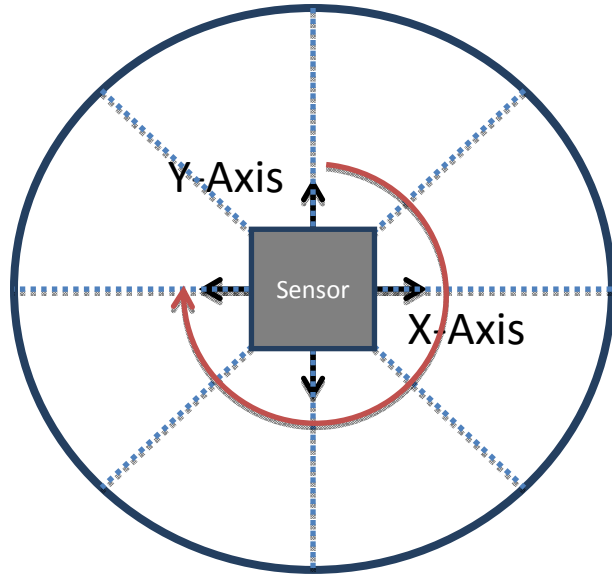
To fix this problem, the amplitude of a given sensor can be modeled as follows:

$$|\vec{B}| = R \times \sqrt{a_x(X - X_{offset})^2 + a_y(Y - Y_{offset})^2 + a_z(Z - Z_{offset})^2} \quad (4.1)$$

In this model, X , Y and Z are the measurements of magnetic sensors in its three dimensions. X_{offset} , Y_{offset} and Z_{offset} represent offsets in the measurements resulting from offsets of magneto-sensitive resistors of sensor and manufacturing asymmetries. Sensitivity of magneto-

sensitive resistors used in three dimensions might differ, and one dimension can show higher sensitivity to the magnetic field. a_x , a_y and a_z are used to represent sensitivity ratios of three axes. For the purpose of uniformity, a_x is set to 1, and the other sensitivity ratios compared to the X-axis are calculated. Finally, R represents the relative overall sensitivity of magnetic measurements of one sensor compared to the other. For example, R of one sensor could be set to 1 as the reference point, and R of other sensors is calculated against it as a relative indicator of magnetic field magnitude.

An experiment was designed to determine the coefficients corresponding to each sensor. Two different sensors of the same type were deployed in similar environmental conditions (location, temperature, etc.), and magnetic field in different directions were measured. As Figure 4-2 shows, while both sensors were rotated 360° , their X-axis, Y-axis and Z-axis values were recorded in each 45° interval. Since both sensors measure same magnetic field, one may assume they will present similar values in all three dimensions. However, due to asymmetry in their sensitivities, different values were reported.



Readings of Two Sensors (X,Y axis) After 360 degree Rotation

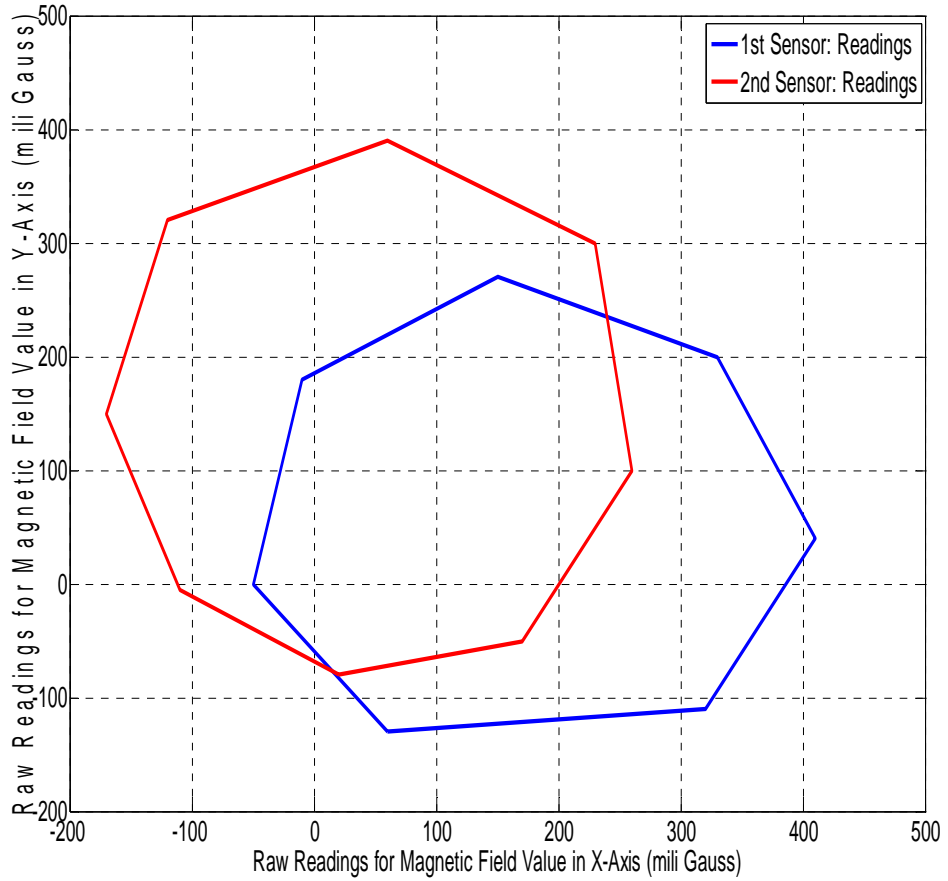


Figure 4-2 : X-Y values for two different sensors after 360 degree rotation

If a sensor is rotated 90° in the X-Y plane, the X-axis of the sensor will be in the direction of the Y-axis before the rotation and the Y-axis will be in the reverse direction of the X-axis before the rotation. Therefore, the after-rotation X value should be equal to the before-rotation Y value, and the after-rotation Y value should be equal to the negative value of the before-rotation X value. This means rotation of the sensor in the X-Y plane should give us a perfect circle with a center at X=0 and Y=0. This is also true if the sensor is rotated in X-Z or Y-Z planes for same reason.

However, as Figure 4-2 shows, rotation of sensors does not yield a perfect circle centered at origin due to offsets and different sensitivities. Using this fact, a calibration method that helps to find the coefficients in Equation 4.1 was developed. Rotation of the sensor in the X-Y, Y-Z and X-Z planes forms an ellipsoid, which should have been a perfect spheroid centered at the origin if there was no offset and all sensitivities of magneto-sensitive resistors in all three dimensions were identical. By mapping the ellipsoid to a spheroid centered at the origin, the following coefficients can be derived:

$$X_{offset} = \frac{X_{maximum} + X_{minimum}}{2} \quad (4.2)$$

$$Y_{offset} = \frac{Y_{maximum} + Y_{minimum}}{2} \quad (4.3)$$

$$Z_{offset} = \frac{Z_{maximum} + Z_{minimum}}{2} \quad (4.4)$$

$$a_x = 1, a_y = \frac{Y_{maximum} - Y_{minimum}}{X_{maximum} - X_{minimum}} a_x \quad (4.5)$$

$$a_x = 1, a_z = \frac{Z_{maximum} - Z_{minimum}}{X_{maximum} - X_{minimum}} a_x \quad (4.6)$$

As mentioned earlier, a_x is set to 1 to measure the comparative sensitivity of Y-axis and Z-axis to X-axis. Similarly speaking, any of the three axes can be chosen as the base axis. To determine the value of R, one sensor is used as the base sensor. Compared to the base sensor, the R-value of other sensors can be determined by dividing the radius of mapped spheroids to the radius of the mapped spheroid of the base sensor at the same location. Following is the equation:

$$R = \frac{\sqrt{a_x(X - X_{offset})^2 + a_y(Y - Y_{offset})^2 + a_z(Z - Z_{offset})^2}}{\sqrt{a_{x_{base}}(X_{base} - X_{offset_{base}})^2 + a_{y_{base}}(Y_{base} - Y_{offset_{base}})^2 + a_{z_{base}}(Z_{base} - Z_{offset_{base}})^2}} \quad (4.7)$$

After calibration, it is expected to have the same results using different sensors in the same conditions. This is crucial in designing the processing algorithm because it must be independent of physical differences between sources of detection. Calibration results for several sensors at different locations were also tested. As Figure 4-3 demonstrates, the calibration does not vary by location and is mostly influenced by the internal parameters such as sensitivity asymmetry and offsets.

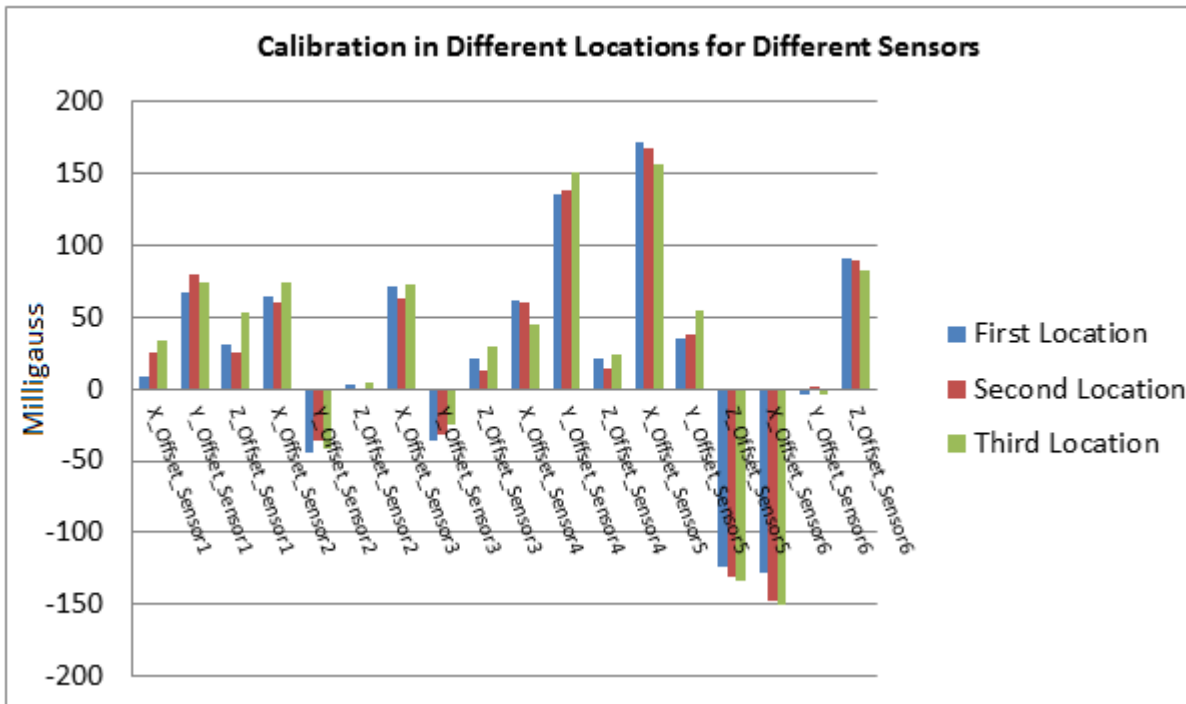


Figure 4-3 : Consistency of calibration results for different sensors in different locations

4.2 Magnetic Field Distribution for Vehicles

In this step, the magnetic fields of vehicles were analyzed, and the intensity of vehicles' magnetic fields in different positions underneath the vehicles was measured. To do this, an array of six sensors with a 13.5-inch separation was designed, and different types of vehicles were scanned for their magnetic field distribution. The goal for this experiment was to measure the distribution of the magnetic fields. Knowledge of such distribution helps determine the best place to install the sensor on the parking spot and helps determine a threshold for the model to decide whether a vehicle is present. Finally, the side effects of vehicles on the neighboring spots were analyzed.

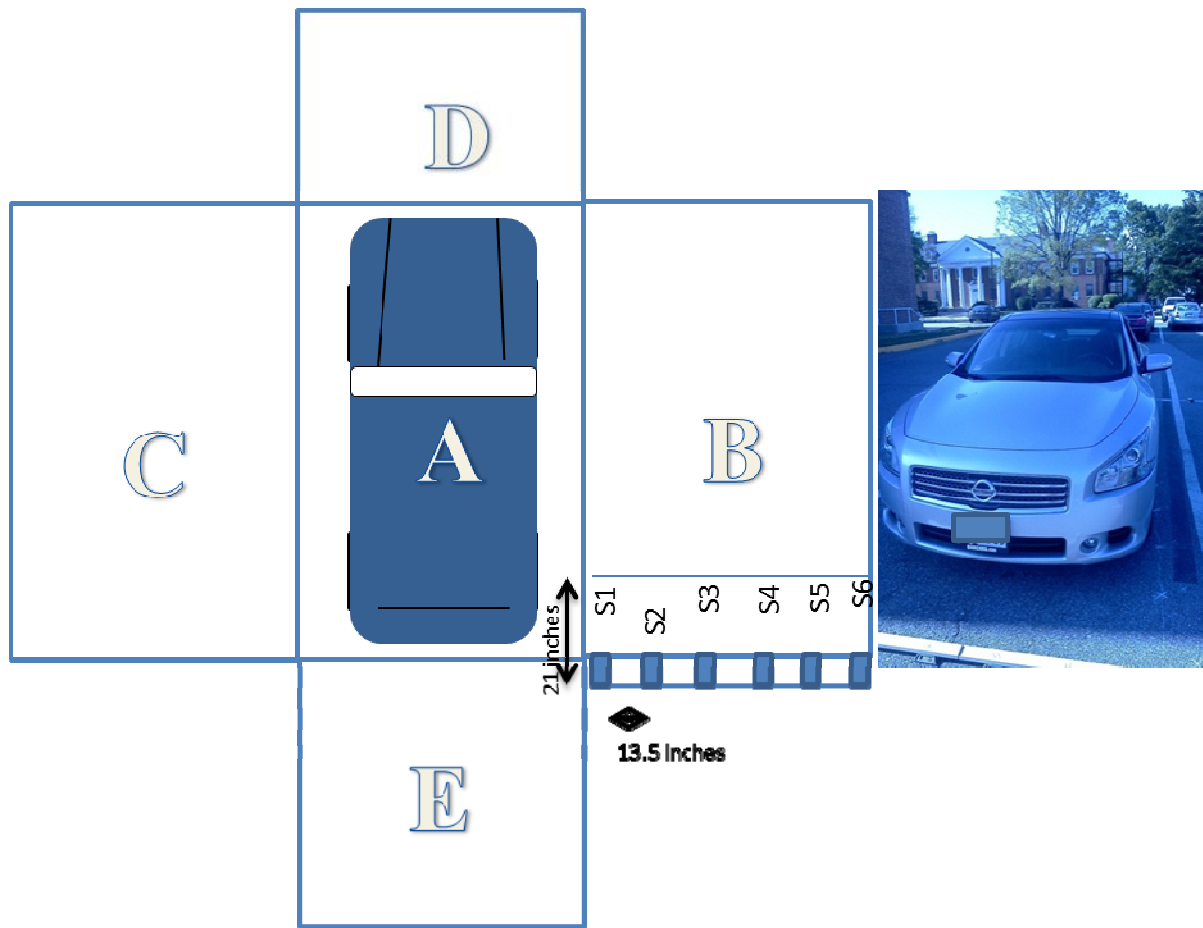


Figure 4-4 : Experiment setup for deriving signature map of the vehicle using array of sensors

Figure 4-4 shows one of the experiment setups on a Nissan Maxima 2011. A system of six sensors with 21 inches separation was used to scan the left, right, front, back, and under side of the vehicle. Results of the experiment are presented in Figure 4-5. As the figure shows, the main magnetic effect of this Nissan Maxima is located toward the front side and within one third of the area underneath the car. This is due to the presence of the engine and also the connection of the axle and steering systems. Similar trends were found over experiments with different types of vehicles.

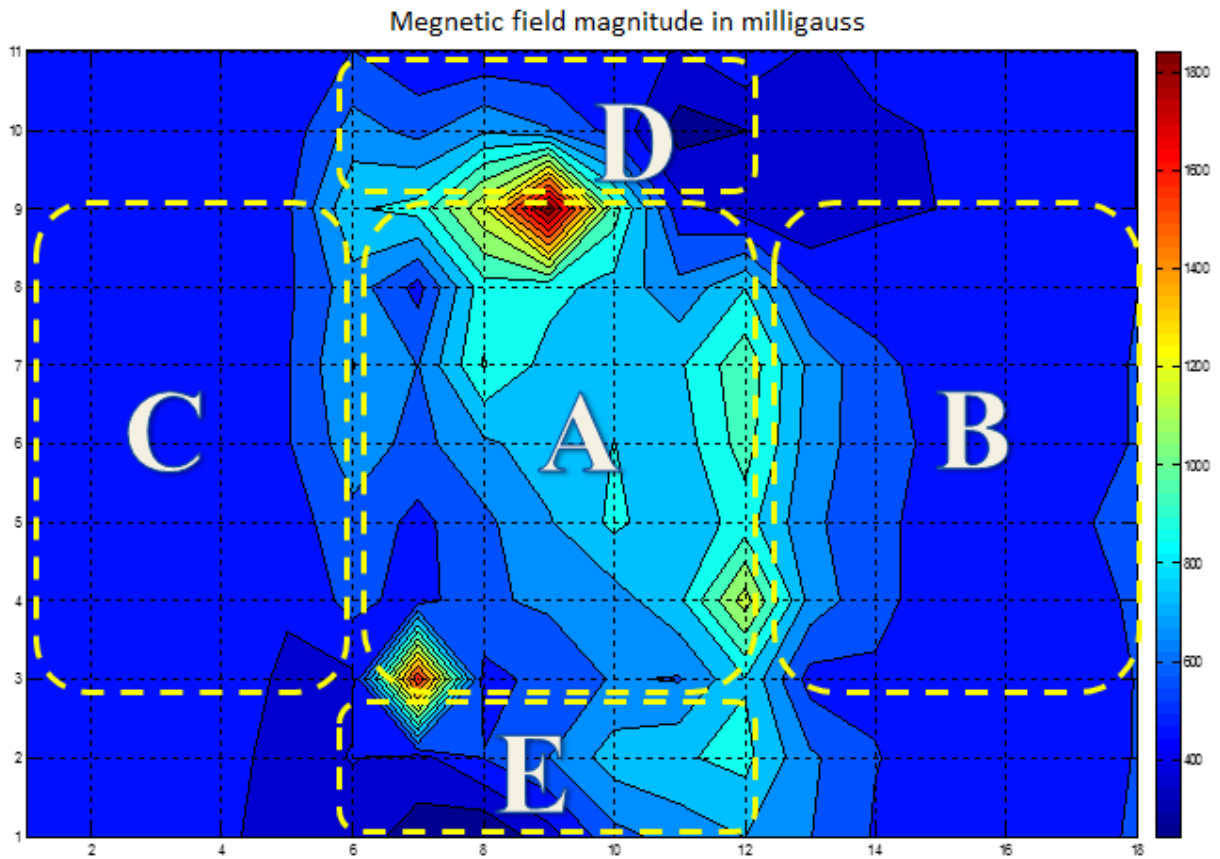


Figure 4-5 : Signature of magnetic field amplitude resulting from underneath a vehicle and its neighboring spots

As illustrated in Figure 4-5, the magnetic effect of the vehicle is not limited to its underneath; the surrounding side area is also affected. This causes one of the major challenges in this project. Since sensors are installed in different spots, one vehicle might induce an interfering magnetic effect on neighboring spots, creating false detection in an empty spot. This challenge is addressed in the next section. Another issue shown in Figure 4-5 is the random distribution of the magnetic field underneath the car due to randomness of relative position of the sensor to the vehicle. Even if a sensor is deployed on a specific point of a spot, a particular car with a known magnetic effect will generate different values if it parks in different manners. Different vehicles

also have different magnetic effects, meaning that Figure 4-6 varies for different vehicles. Therefore, there are two sources of randomness that calls for non-deterministic decision-making.

Vehicles of different makes and models were tested, and results show that the area covered by a one-third section of the car on the driver side is the best place for sensor installation since one can statistically expect the highest magnetic effect at that point. Considering the cross-magnetic effects mentioned earlier, the middle line of the spot in the direction of parking is the best place to avoid unwanted magnetic effects from the neighboring spots. If the direction of parking is arbitrary for the driver, two sensors can be installed on the first and last one-third portion of the spot to address reverse the parking direction problem. Figure 4-6 illustrates the proposed deployment layout.

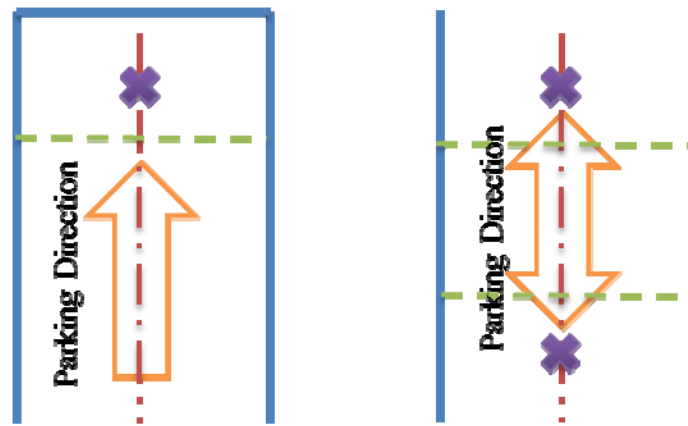


Figure 4-6 : Location and number of sensors to be installed on parking spots

4.3 Temperature Drift and Magnetic Cross Interference

One of the challenges in using magnetic sensors is sensitivity to temperature. Since resistance of magneto-sensitive sensors is temperature dependent, even without any change in magnetic field

they can report different values with the variation of temperature. Figure 4-7 demonstrates this variation for a daylong deployment.

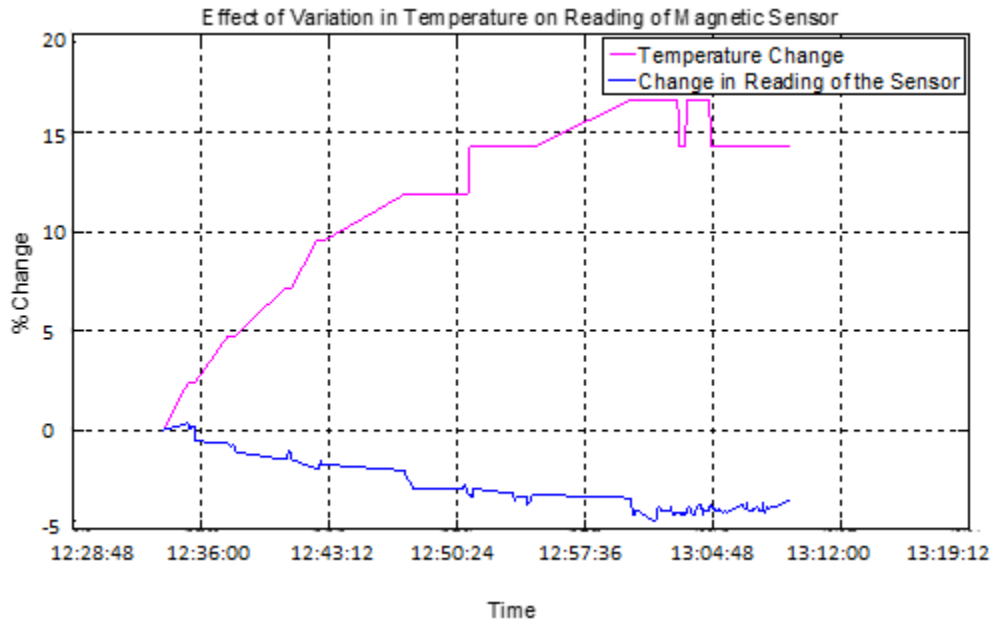


Figure 4-7 : Effect of temperature drifts on reading of sensors

Figure 4-8 shows that as the temperature increases, the sensitivity of reading in the sensor also increases. This explains the considerable variation in magnetic value reported by the sensor in Figure 4-7 over a range of temperature points. This could be an important issue, especially when the temperature changes significantly during the system operation. The research team developed equations for compensating temperature drift that relies on recalculating all values of X axis, Y axis and Z axis based on their initial value at an initial temperature. It can be calculated using the following equations:

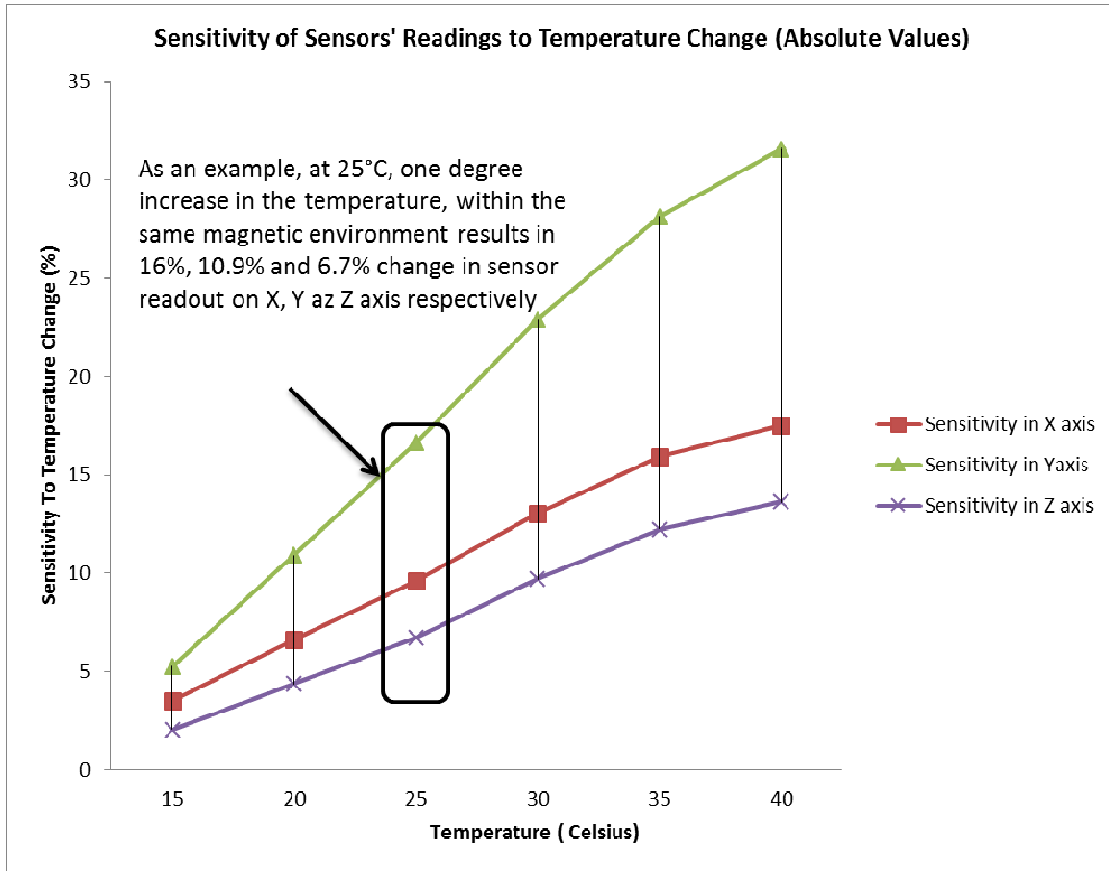


Figure 4-8: Experiment results for calculation of temperature sensitivity in different axes

$$X(Temp = T_0) = X(Temp = T) * e^{0.006(T-T_0)} \quad (4.8)$$

$$Y(Temp = T_0) = Y(Temp = T) * e^{0.008(T-T_0)} \quad (4.9)$$

$$Z(Temp = T_0) = Z(Temp = T) * e^{0.02(T-T_0)} \quad (4.10)$$

Since the CC2530 microcontroller sports a temperature sensor, at each time the X, Y and Z value are received at a temperature equal to "T", they can be adjusted relative to temperature "T₀".

After temperature compensation and data smoothing, results are shown in Figure 4-9. This filter avoids rapid changes in the magnetic field data due to temperature jumps.

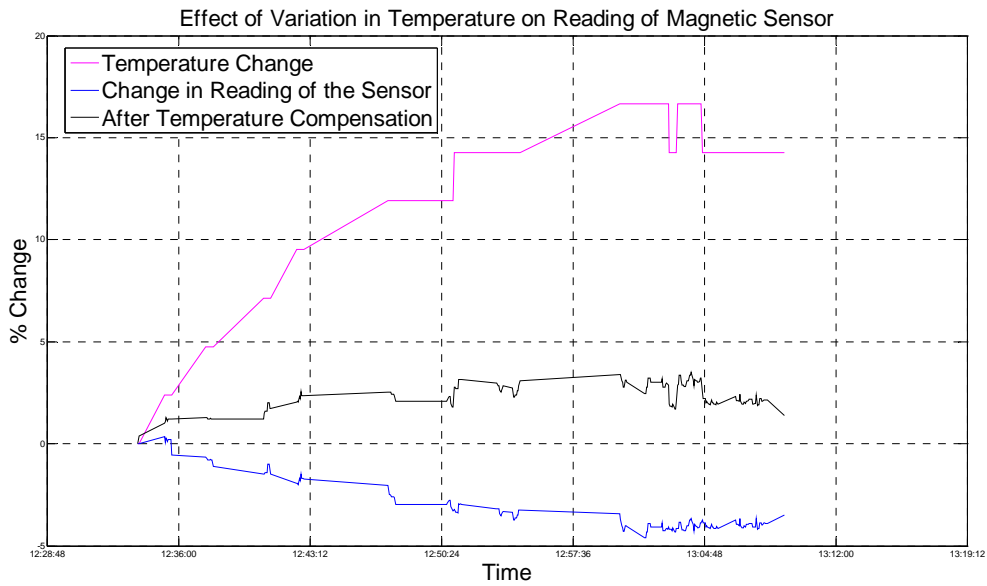


Figure 4-9 : Compensation of temperature drifts

Interference of several magnetic fields existing in any environment might have major effects on the reading of sensors, and this is a major issue in using magnetic sensors. One of the most common situations in which interference causes false detection is when a vehicle parks on a particular spot but concurrently disturbs the magnetic field of its neighboring spots. To address this issue, the cross-effects of vehicles were examined as a way to find a relationship between their individual and mutual effects on sensor readings. Setup for these experiments is illustrated in Figure 4-10.

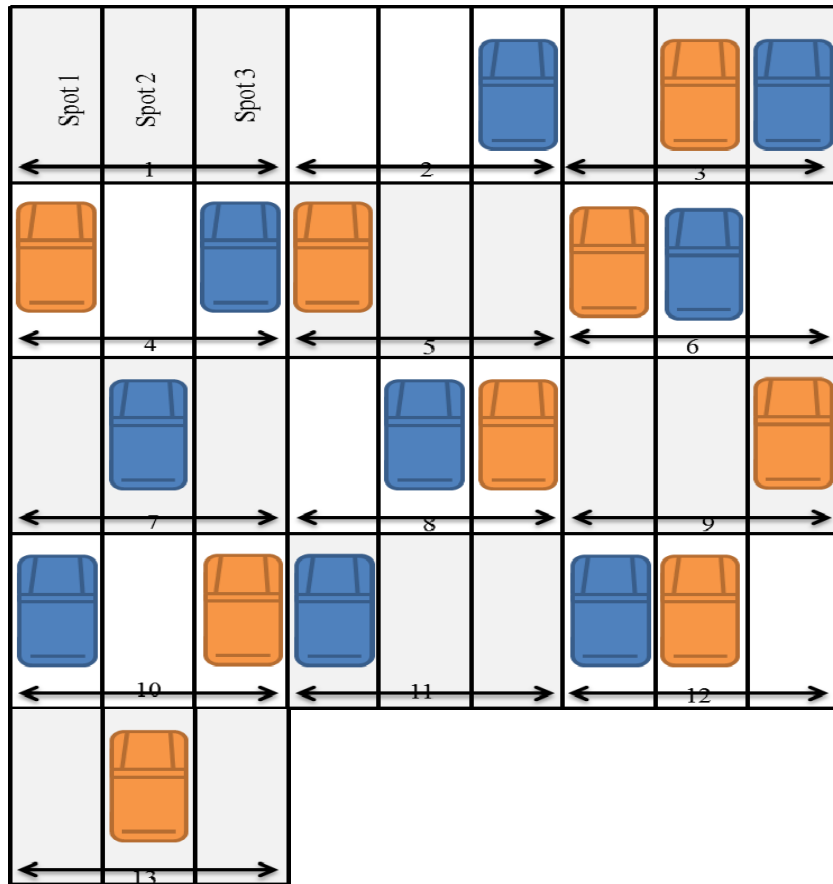


Figure 4-10 : Experiment setup to check linearity effect of neighboring spot's magnetic field interference

In this setup, 13 scenarios using two vehicles were designed. Scenarios were created by changing the location of vehicles in three neighboring spots covered by three sensors (one sensor in each spot.) After reading and analyzing the data of each sensor, linearity in the mutual effects of the vehicles was detected. In other words, the mutual effect of two cars is the summation of the effect of each when the other one does not exist. Results of Scenarios 1, 2, 3 and 13 based on the layout presented in Figure 4-10 are summarized in Table 4-1.

Table 4-1 : Experiment Results for Linearity of Cross Interference Effects

| | Scenario 1 | Scenario 2 | Scenario 13 | Scenario 3 |
|-------------|------------|------------|-------------|------------|
| X_{Spot1} | 56.213 | 59.1746 | 126.1528 | 128.241 |
| X_{Spot2} | 45.537 | 87.463 | 56.1944 | 137.583 |
| X_{Spot3} | 26.5093 | -251.7222 | 5.6914 | -265.9 |
| Y_{Spot1} | 247.6136 | 242.3252 | 227.8736 | 222.707 |
| Y_{Spot2} | 344.4185 | 323.7814 | -0.4256 | -75.559 |
| Y_{Spot3} | 321.3153 | 248.5808 | 309.9128 | 237.658 |
| Z_{Spot1} | 470.1164 | 467.5446 | 465.9411 | 465.147 |
| Z_{Spot2} | 450.8576 | 439.2385 | 571.9482 | 662.005 |
| Z_{Spot3} | 571.5362 | 906.7534 | 555.1056 | 879.319 |

In Scenario 1, no vehicle is present; thus, it is considered as base case. To derive the individual effect of each of the two vehicles on each spot, subtract their recorded values in Scenario 2 and Scenario 3 from the base case (Scenario 1). To derive the mutual effect of both vehicles on each spot, the collected data of Scenario 3 was subtracted from the base case. For example, having checked the collected data for the X-axis of the sensors installed on the first spot, the sum of the individual effects is almost the same as the mutual effect for the X-axis:

$$\text{Sum of Individual Effects} = (X_{Spot1}^{Scenario2} - X_{Spot1}^{Scenario1}) + (X_{Spot1}^{Scenario13} - X_{Spot1}^{Scenario1}) = 72.90$$

$$\text{Mutual Effects} = (X_{Spot1}^{Scenario3} - X_{Spot1}^{Scenario1}) = 72.028$$

Figure 4-11 demonstrates the results for other axes and spots. As the figure shows, the sum of the individual effects for each of two tested vehicles generates an effect equal to the effect of the case when both of the cars are parked. This means that by knowing a vehicle is parked on a

particular spot, its cross-effect can be extracted from the neighboring spots. In other words, by reducing the changes in the X-, Y- and Z-axes made by a detected event at the neighboring spots the pure magnetic field value for a given spot can be estimated. This result is utilized in developing the processing algorithm.

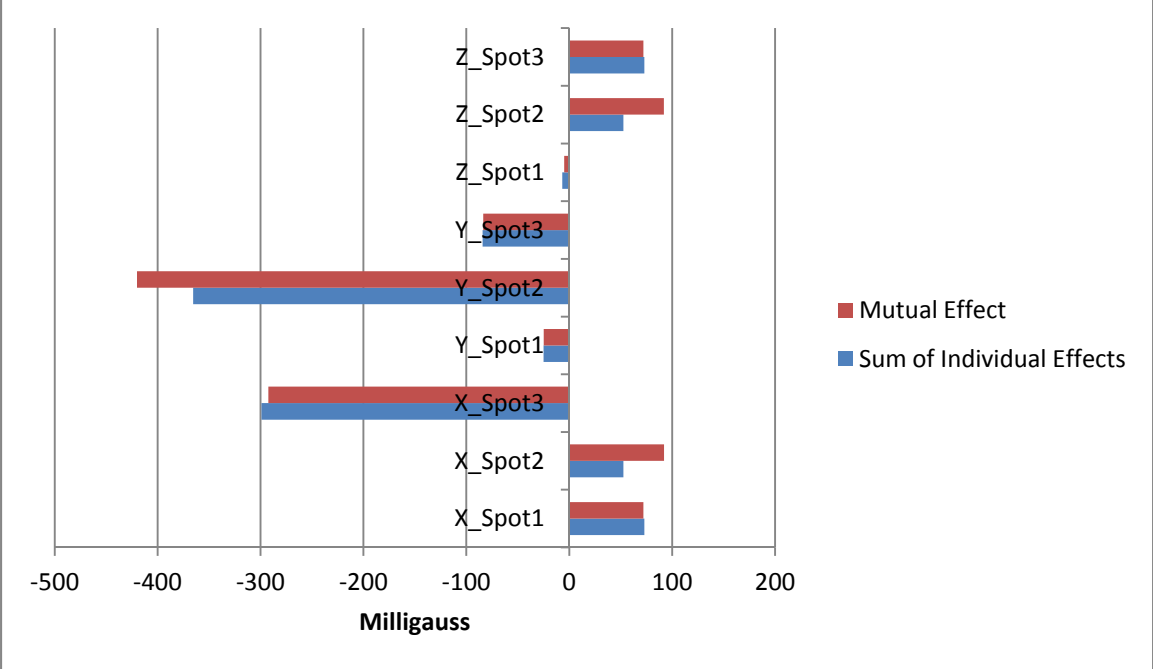


Figure 4-11 : experiment results showing linearity effects

4.4 Processing Algorithm

At this step, having gained enough understanding of the magnetic fields measured by the sensors, the magnetic effects of different type of vehicles and the environmental effects (such as temperature drifts or cross interferences) on sensor reading, the research team designed a processing algorithm to detect the presence of vehicles. In the processing algorithm, both the calibration information of the sensors and the topology of the sensors installed in the field were

considered. As mentioned earlier, calibration information is necessary to make the readings of different sensors as uniform as possible. Topology of the network is also necessary to inform the processing algorithm about the location of the sensors and to compensate for the cross-interferences. Using statistical analysis on the magnetic signature of different vehicles, required magnetic field thresholds were set to cluster the sensors' measurements and make the decisions about the status of the spots. The processing algorithm was designed with two options of memory-less and memory-based as the flowchart in figure 4-12 shows.

In the memory-less processing, the information of past events in the network of sensors is not required to detect the current status of the network. On the contrary, in memory-based approach the previous status is provided as feedback to the system for determining its current status. Memory-less approach could be used in cases in which cross-interferences are not dominant. This case is more common when a parking lot is designed in a way that there are enough spaces for the vehicles and where drivers park very precisely in their own spots. In memory-based processing, cross-interferences are too high to be ignored, and a history of the status of all spots should be used and continuously updated. Memory-based processing is more precise, but it needs very accurate initialization of the system, which takes much more processing effort compared to the memory-less processing.

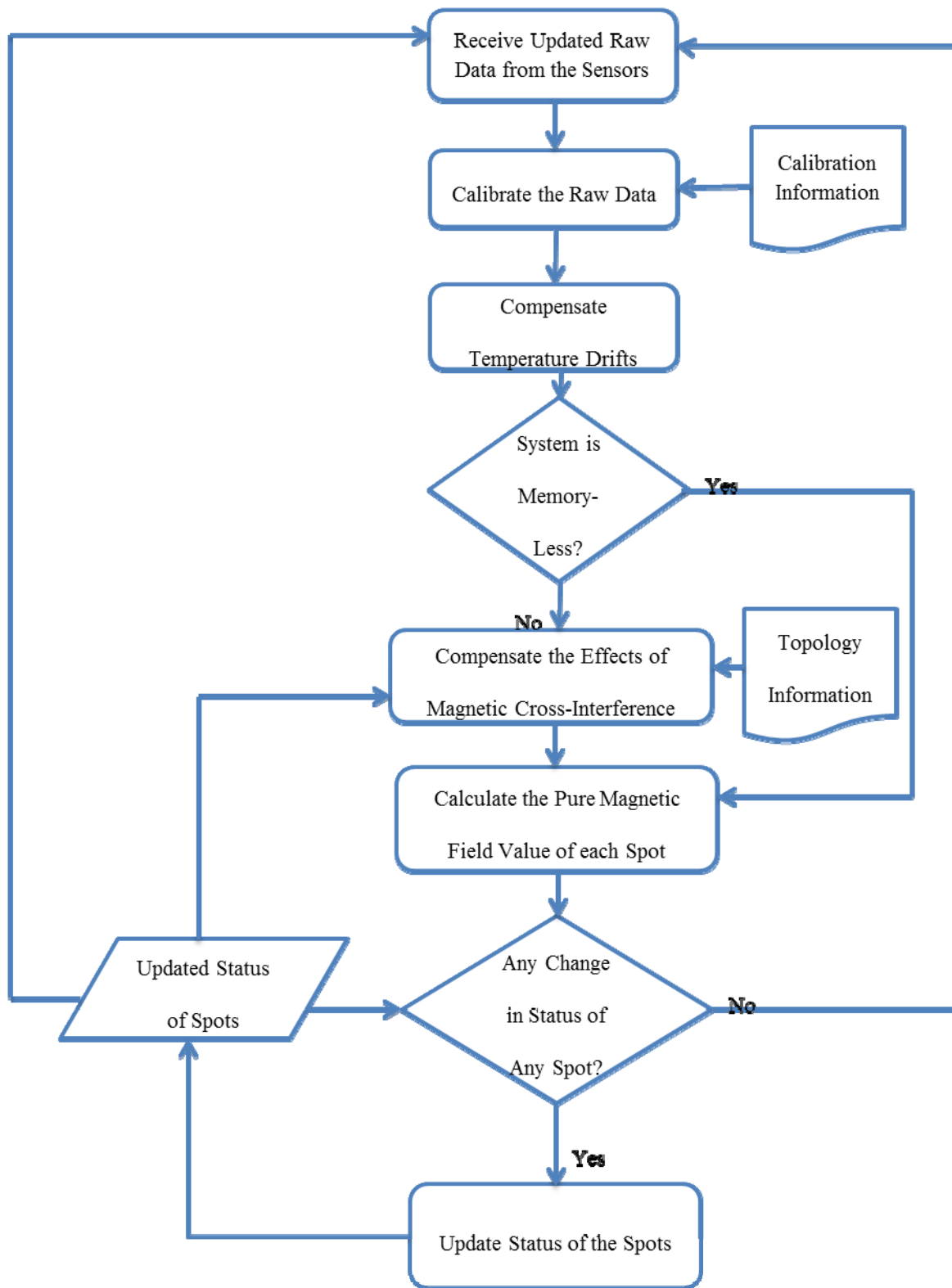


Figure 4-12 : Flowchart of processing algorithm

After the calibration and compensation for temperature drifts (and compensation for cross-interferences in case of memory-based processing), pure magnetic field values on top of each sensor can be estimated. To determine the status of each spot, the pattern of the pure magnetic field for that spot during a reasonably selected time window should be monitored. Using supervised learning algorithms, the team designed a clustering scheme to check the pattern of the magnetic field (after compensation) .In the case of any change in the status, an update will be sent to the servers. For clustering, some threshold values should be determined from supervised learning algorithms. The values may be customized for any parking lot to optimize the system’s overall performance.

Let’s consider the status of spots to be represented by \vec{s} , which is a binary vector with a length equal to the number of spots. The reading of sensors is represented by \vec{r} , which is a vector with a length equal to the number of sensors. The goal of the learning algorithm is to find a parameterization scheme based on the training samples (a combination of ground truth data and collected data) represented by $\vec{\theta}$, to maximize the likelihood of correct prediction of the spots’ statuses. In other words, $\vec{\theta}$ that maximizes $(\vec{s} | \vec{r}; \vec{\theta})$ must be calculated.

As an example, consider the case in which two spots are monitored by two sensors. As illustrated in Figure 4-13, a set of parameters can be obtained by using the learning algorithm, which can be used to classify the readings of two sensors into four areas, each representing one value for status vector. After determining the cluster in which the sensors’ reading belongs to, the status of spots will be estimated and updated at any given time.

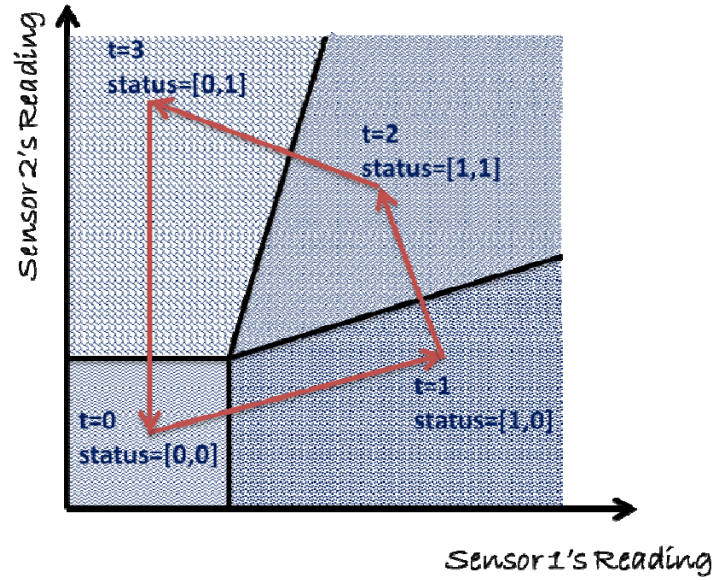


Figure 4-13 : A clustering example for two spots monitored by two sensors

For the cases in which more than one sensor is installed in each spot and each sensor reads more than one value (for example X-axis, Y-axis, Z-axis and Temperature), the learning algorithm can be generalized with the following:

$$\text{Find } \vec{\theta}_{nk \times m} \text{ that } \frac{\partial P(\vec{S}_{m \times 1} | \vec{R}_{nk \times 1}; \vec{\theta}_{nk \times m})}{\partial \vec{\theta}_{nk \times m}} = 0 \quad (4.11)$$

In Eq. 4.11, m is the number of spots, n is number of sensors and k is number of the sensor's parameters. After receiving and processing enough numbers of training samples, $\vec{\theta}_{nk \times m}$ is calculated. Based on that vector, the status of each spot can be estimated by mapping the readings of sensors into a multidimensional space. Figure 4-13 shows an example of a case with

two dimensions. Based on clustering derived from a parameterization function $h_{\theta} \left(\begin{matrix} \rightarrow \\ R_{nk \times 1} \end{matrix} \right)$, the status of spots $\left(\begin{matrix} \rightarrow \\ S_{m \times 1} \end{matrix} \right)$ is estimated:

$$\begin{matrix} \rightarrow \\ S_{m \times 1} \end{matrix} = h_{\theta} \left(\begin{matrix} \rightarrow \\ R_{nk \times 1} \end{matrix} \right) \quad (4.12)$$

Where $h_{\theta} \left(\begin{matrix} \rightarrow \\ R_{nk \times 1} \end{matrix} \right)$ is generated from the parameterization vector $\left(\begin{matrix} \rightarrow \\ \theta_{nk \times m} \end{matrix} \right)$.

Parameterization function used for the decision-making algorithm is a logistic function described in Equation 4.13.

$$h_{\theta} \left(\begin{matrix} \rightarrow \\ x \end{matrix} \right) = \frac{1}{1 + e^{-\theta^T x}} \quad (4.13)$$

Assuming only one spot to be monitored ($m=1$), the one-dimensional logistic function is plotted in Figure 4-14.

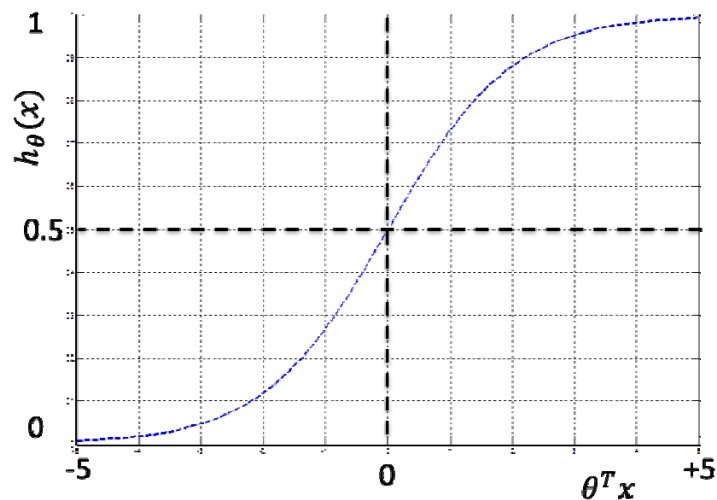


Figure 4-14: Logistic function for one spot

If the value of the status of the i^{th} spot resulted from Equation 4.12 is greater than 0.5, the status of the spot is estimated to be occupied because $P(S_i = 1 | \vec{\rightarrow}_R; \vec{\rightarrow}_\theta)$ is greater than $(S_i = 0 | \vec{\rightarrow}_R; \vec{\rightarrow}_\theta)$.

The probability of detection error is smaller if the value derived for the elements of $\vec{\rightarrow}_{S_{m \times 1}}$ is close to either 0 or 1. Probability of error is related to the variance of inputs ($\vec{\rightarrow}_R$), which are the readings of the sensors installed on the spots. The variance of the sensors' readings for different events depends on the variation of the magnetic field distribution of the vehicles (discussed in Section 4.2). It also depends on how precisely drivers park on the marked spots and follow the layout.

In all equations 4-11 to 4-13, the decision-making was memory-less. In other words, the status of spots was not dependent on the history of the events and readings in the past. However, to reduce the effects of cross-interference, which increases the error rate in cases that the drivers do not park very precisely and the spots are too close to each other, a memory-based algorithm is designed. In the memory-based algorithm, instead of maximizing $(\vec{\rightarrow}_S | \vec{\rightarrow}_R; \vec{\rightarrow}_\theta)$, the $P(\vec{\rightarrow}_S^{t+1} | \vec{\rightarrow}_R^{t+1}; \vec{\rightarrow}_R^t; \vec{\rightarrow}_S^t; \vec{\rightarrow}_\theta)$ should be maximized. Here, the linearity of mutual effects of vehicles on neighboring spots (discussed in Section 4.3) can be applied to make the processing algorithm less complex and more reliable. To do so, a new modified variable ($\vec{\rightarrow}_{R_m}^{t+1}$) can be defined as

follows:

$$\vec{\rightarrow}_{R_m}^{t+1} = \vec{\rightarrow}_R^{t+1} + (T_{nk \times m} \times \vec{\rightarrow}_{S_{m \times 1}}^t \times L_{1 \times nk}) \times \vec{\rightarrow}_R^t \quad (4.13)$$

T is the topology matrix used to distinguish the neighboring spots, and L works as a function that, based on the status of the neighboring spots, applies the linearity and compensates the cross-

interference effects of magnetic fields. Using this new modified variable, the same equations used in the memory-less algorithm can be applied to find the status of the spots:

$$\text{Find } \vec{\theta}_{nk \times m} \text{ that } \frac{\partial P(\vec{s}_{m \times 1} | \vec{R}_{m_{nk \times 1}}; \vec{\theta}_{nk \times m})}{\partial \vec{\theta}_{nk \times m}} = 0 \quad (4.14)$$

$$\vec{s}_{m \times 1} = h_{\theta} \left(\vec{R}_{m_{nk \times 1}} \right) \quad (4.15)$$

Although the memory-based algorithm theoretically leads to lower error rates since it reduces the cross interference effects, it is sensitive to the accuracy of predictions in the past. An error in detection of an event due to a signaling block can be propagated in other spots until the error is removed. To solve this problem, a time window can be designed to make sure there is enough data from all the neighboring spots to apply the modifications. The downside of this approach is that it increases the delay in the decision-making. A possible solution is to increase the sampling rates of the sensors, which consumes more power and is less efficient.

As a conclusion, the memory-based algorithm obtains better error rates but has costs of more complexity, higher delay in response time and higher power consumption. The memory-based algorithm is a good alternative when high accuracy data is available or the dynamics of the parking lot and behavior of drivers diminishes the functionality of memory-less algorithm.

4.5 Testing and Modifications

A pilot deployment was done on a selected SHA's truck parking facility (located on northbound I-95 prior to MD-32) in January 2013. Approximately 5Gbytes of sensors' measurement data along with ground-truth images were received in the first 30 days. All data were captured by a collector and directly forwarded to the data center at UMD's traffic sensors laboratory.

Necessary modifications were applied after processing the received data and analyzing the performance of the system. Based on the results, a customized algorithm for truck parking information was finalized.

In the selected facility, most of the drivers respected the parking layout and parked between lines. Also, the spots were rather wide, which made the cross-interferences less destructive to data accuracy. Thus, the memory-less algorithm delivered acceptable results. Although most of the trucks occupied the entire spot, some smaller trucks or trucks without trailers parked in the facility, which covered only a portion of the spot. Each spot was equipped with two sensors to cover these cases.

Figure 4-14 is an example of the data processing with two sensors in one spot for a 30-hour period. As the figure shows, in some cases an event could not be detected by only one sensor because the truck did not impose enough magnetic effect on the particular spot. The camera in data collector provided continuous snapshots of the target parking spots as base data. Since an image-based ground-truth was incorporated into the system, detection error can be accurately measured. The green line in the graph shows the ground-truth.

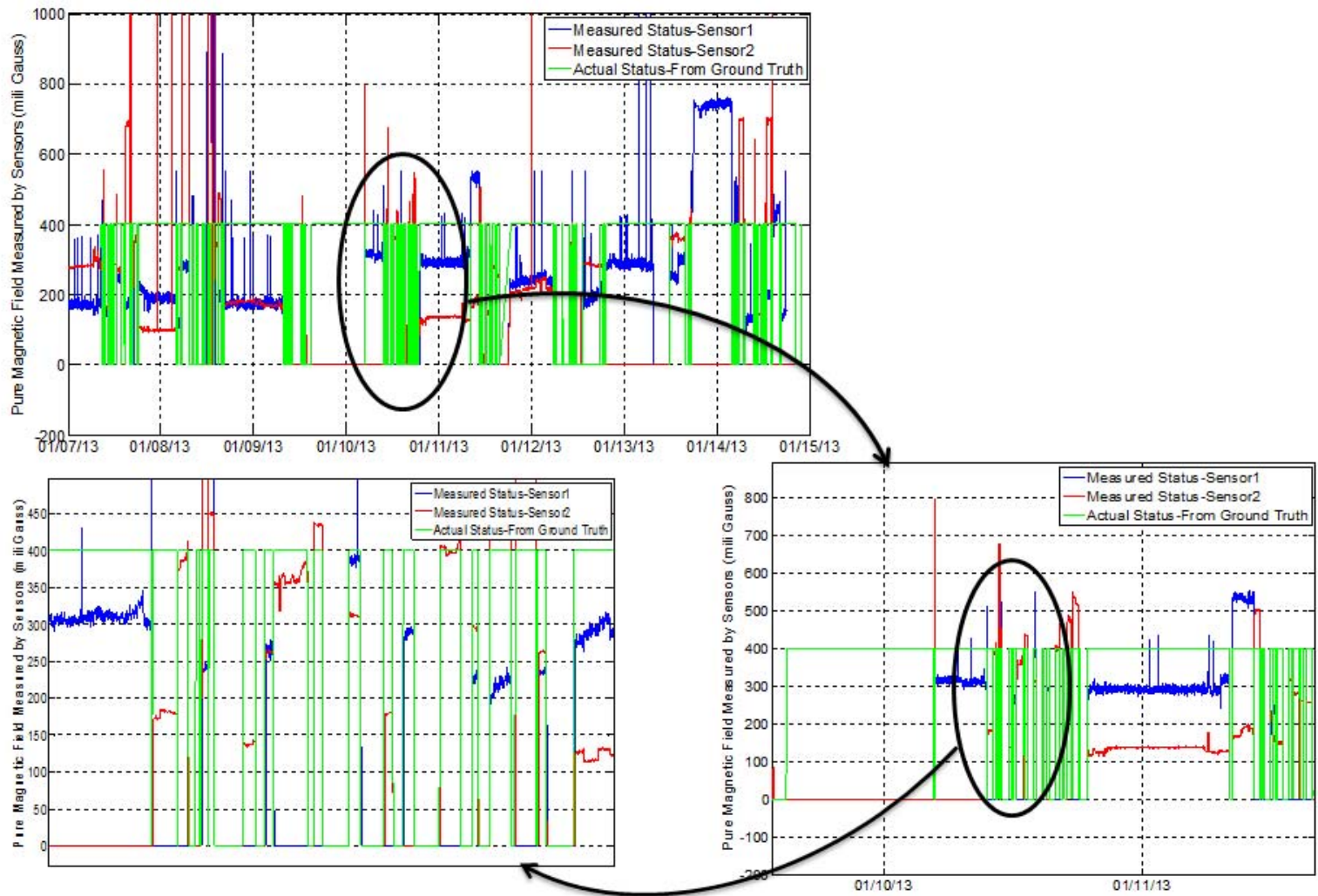


Figure 4-155: Validation of algorithm results with ground truth data

5 Distributed Data Processing

The overall performance of the system was tested and some event reports were produced by installing sensors with different sensitivity levels and different types of antennas on five spots of the truck parking. Figure 5-1 illustrates the experiment setup on the truck parking. For this experiment, two types of sensors (highly sensitive and less sensitive) and two types of antennas (patch antenna and monopole antenna) were tested. One sensor was installed on Spot 1 with a patch antenna and a highly sensitive sensor. The sensor used in this spot used the enclosure design described in Section 2-1-5. This sensor was also implanted in the asphalt and its case was protected with silicon (see Figure 5-2). The antenna of this sensor (patch antenna) is highly directive, meaning that if it has a line of sight to the receiver, a high link quality would be expected. However, in case of signal block, it provides relatively poor quality compared to monopole antennas.



Figure 5-1 : Experiment setup on truck parking field

One sensor with a monopole antenna was installed on Spot 2 with lower sensitivity than the sensors installed on Spot 1. The goal was to compare the performance. Although high-sensitivity sensors show better reactions to even small changes in the magnetic field, they suffer from temperature drifts and cross interferences.

In Spot 3, one sensor with high sensitivity and one with lower sensitivity (both using monopole antenna) were installed. Two highly sensitive sensors with patch antenna were used for Spot 4, and two sensors with patch antenna (one with higher sensitivity and one with lower sensitivity) were used for Spot 5. A summary of experiment setup is detailed in Table 5-1.

Table 5-1 : Experiment setup details

| | Number of Sensors Installed | Number of Highly Sensitive Sensors | Number of Monopole Antennas used | Number of Patch antennas used |
|---------------|------------------------------------|---|---|--------------------------------------|
| Spot 1 | 1 | 1 | 0 | 1 |
| Spot 2 | 1 | 0 | 1 | 0 |
| Spot 3 | 1 | 1 | 2 | 0 |
| Spot 4 | 2 | 2 | 0 | 2 |
| Spot 5 | 2 | 1 | 0 | 2 |

Figure 5.2 shows the installation efforts. Having installed seven sensors on these five spots, collected data was processed; concurrently, ground-truth data was collected to measure the performance of the system in terms of error rate.

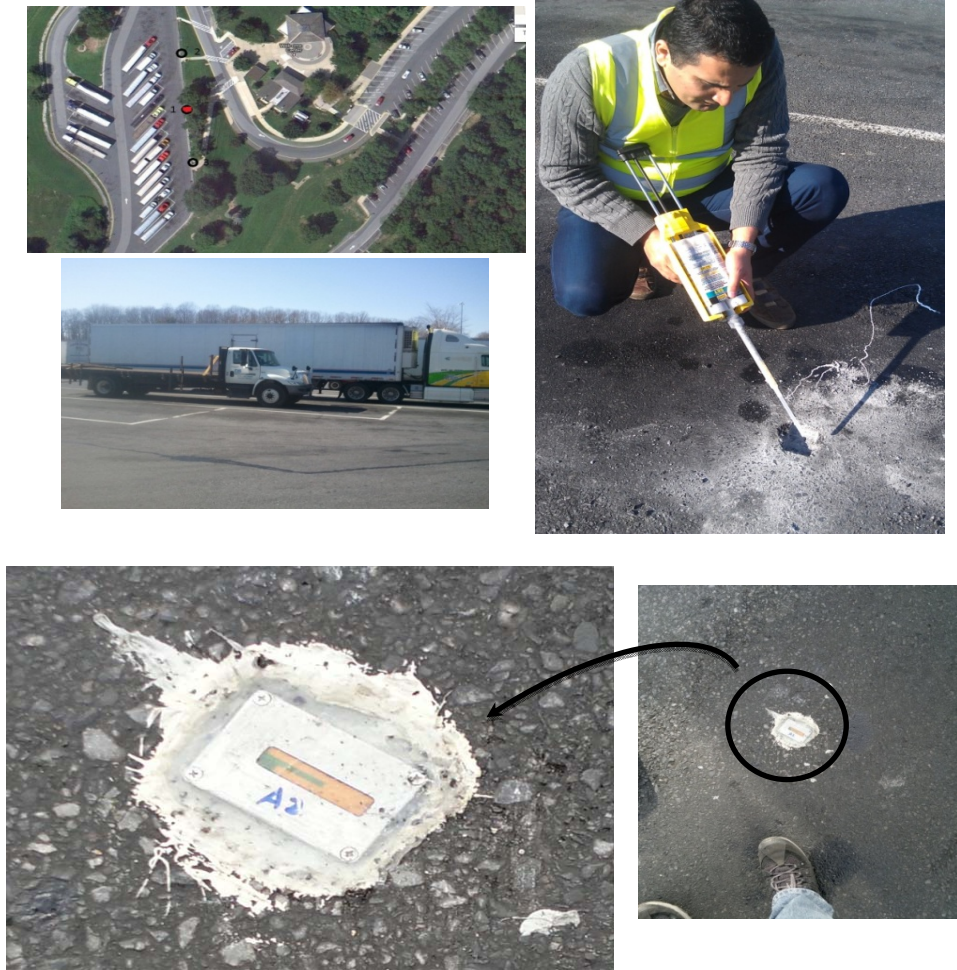


Figure 5-2: Deployment of sensors on truck parking field

Every one second, each sensor measures and transmits the magnetic field through the short-range wireless standard of IEEE 802.15.4. However, due to signal blocks, path loss, multi-path fading, shadowing and electromagnetic interferences, not all packets reach the data collector. The packet loss rate for each spot is demonstrated in Figure 5-3.

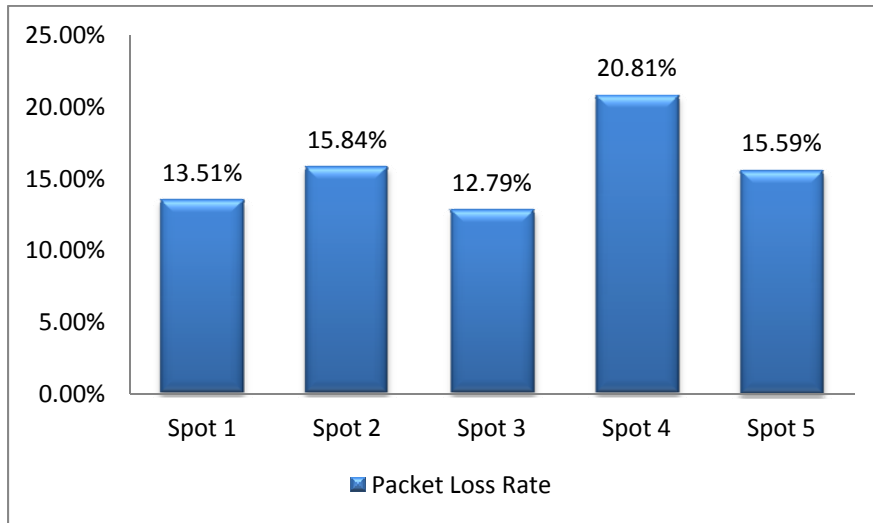


Figure 5-3: Packet loss ratio for each spot

During the testing period between January 6, 2013, until January 14, 2013, 1239 events were detected by the system in all five spots. “Event” refers to any activity of arrival or departure of a vehicle in a spot. As demonstrated in Figure 5-4, some spots experienced fewer events than others. Detailed investigation of the events may help understand why some spots experienced fewer activities. For example, on Spot 5, a single event lasted for three days, which means the spot was occupied by one truck for three days.

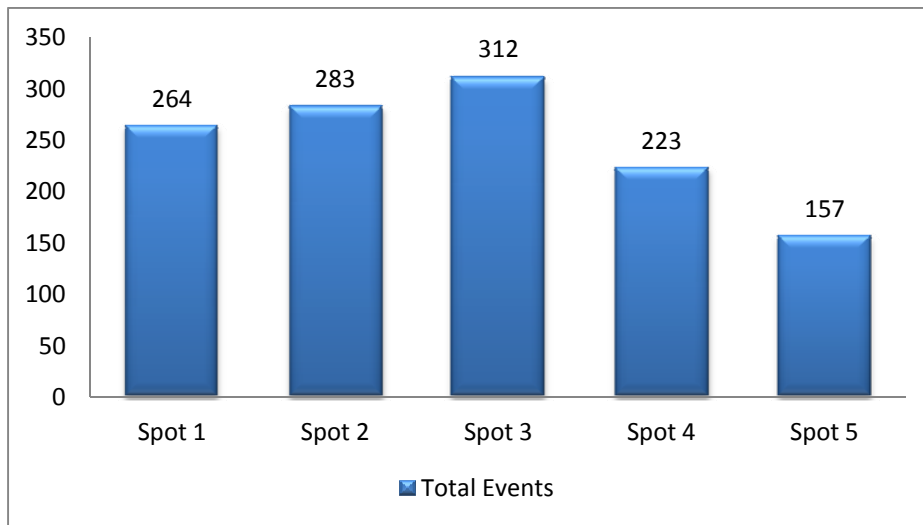


Figure 5-4 : Number of events detected during experiment

The occupancy ratio for each spot is demonstrated in Figure 5-5. Some spots were more utilized during the experiment. For example, Spot 5, which experienced the least number of events, was more occupied than the others since the spot was occupied by one single truck for almost three days. The occupancy ratio of different spots can be monitored with the developed system in real time to control traffic in the parking facilities.

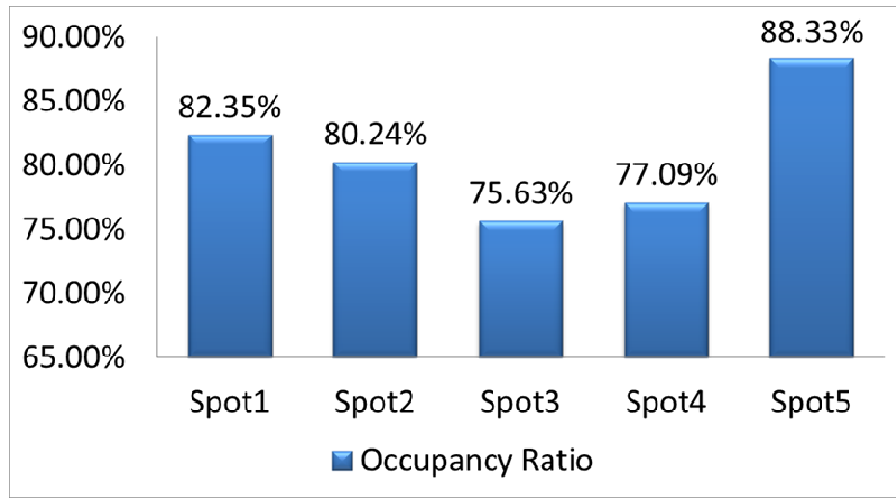


Figure 5-5: Occupancy ratio of different spots during experiment

By comparing the detection results against ground truth data captured by a camera every one minute, the error rate ratio was analyzed. “Error” refers to the number of cases in which a vehicle is detected by the sensors where there was no vehicle detected by the camera (false detection) or cases in which a vehicle was detected by the camera but not detected by any of the sensors. “Error rate” refers to the percentage of the time in which an error was experienced by the system.

Figure 5-6 demonstrates actual status of system and measured status of the system for Spot 1 for one day. The big dark circle highlights a case of detection error analysis. In this case, a vehicle was parked on Spot 1 according to the camera feed represented by the green line. However, the sensor installed on that spot, represented by the blue line, did not detect a truck. The bottom part of the figure zooms on the error case for detailed presentation.

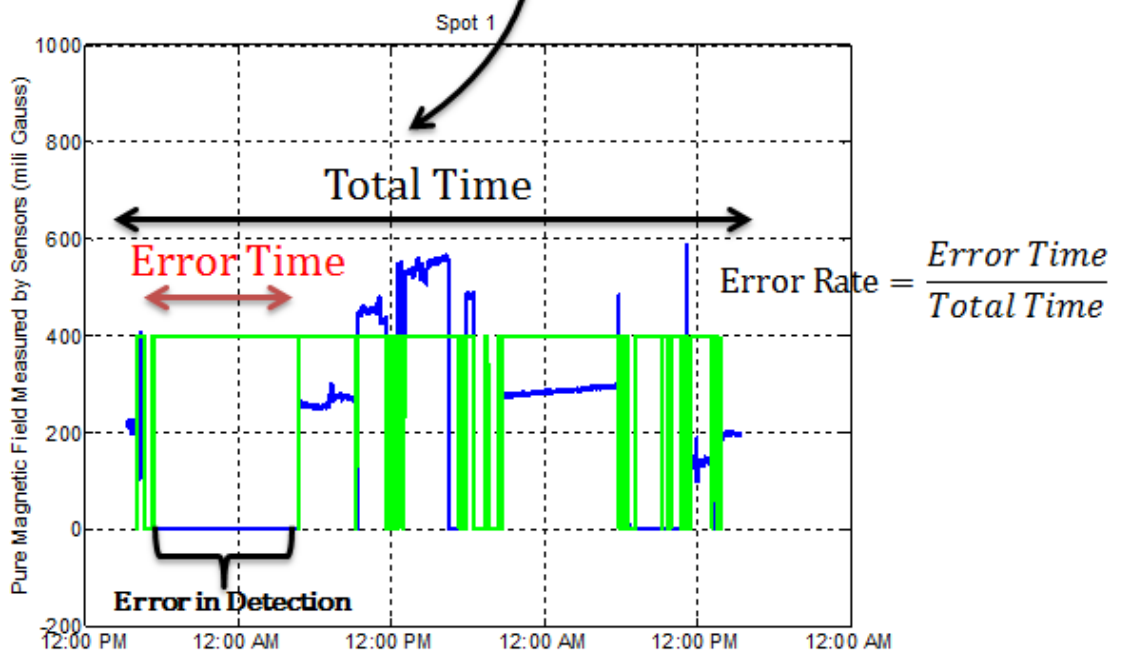
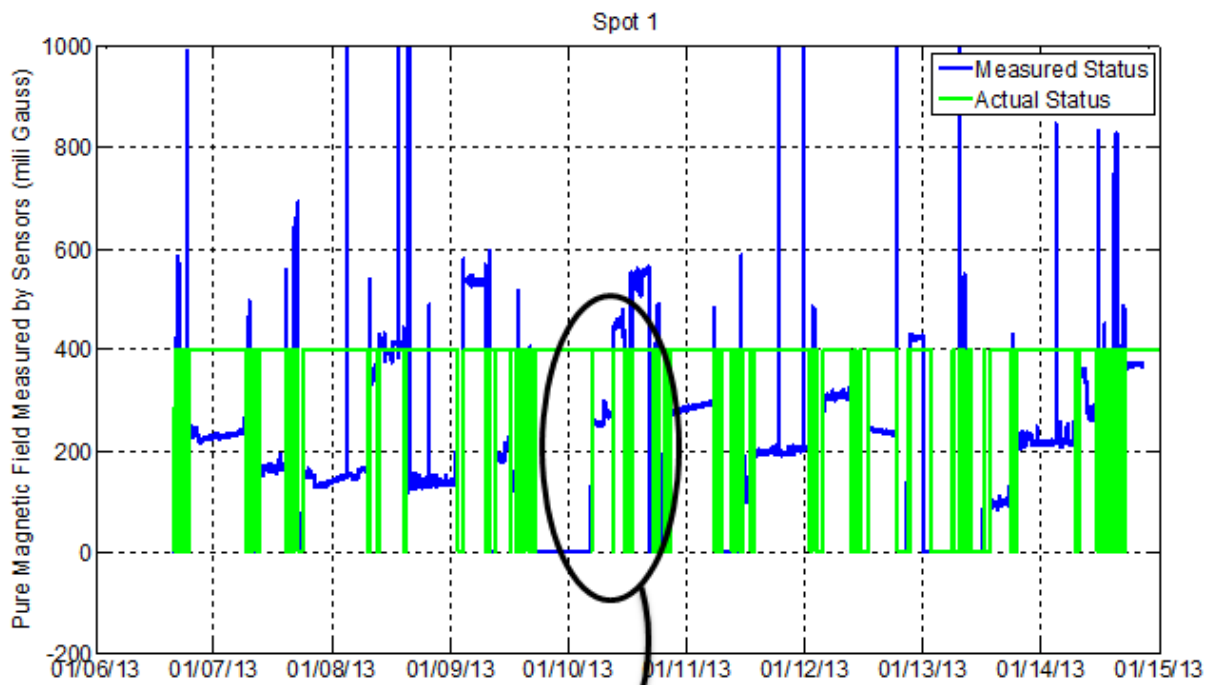


Figure 5-6 : An example for error rate calculation

Figure 5-7 compares error rates for different spots during eight days of experiment. This graph shows that during these eight days, the system measured the status of Spot 1 correctly 94.18 percent of time. The average error rate for all five spots was 3.75 percent. One of the most important findings during this test period is the relationship between error rate and type of sensor and antenna installed on each spot. For Spot 4, in which two highly sensitive sensors with patch antenna were installed, the least error rate was recorded and is considerably lower than Spot 1 where only one highly sensitive sensor and patch antenna were installed. Spot 2, which used only one low-sensitive sensor and a monopole antenna, experienced the highest error rate. Comparing Spot 3 and Spot 5, it is observed that patch antennas had better performance than monopole antennas for this truck parking area.

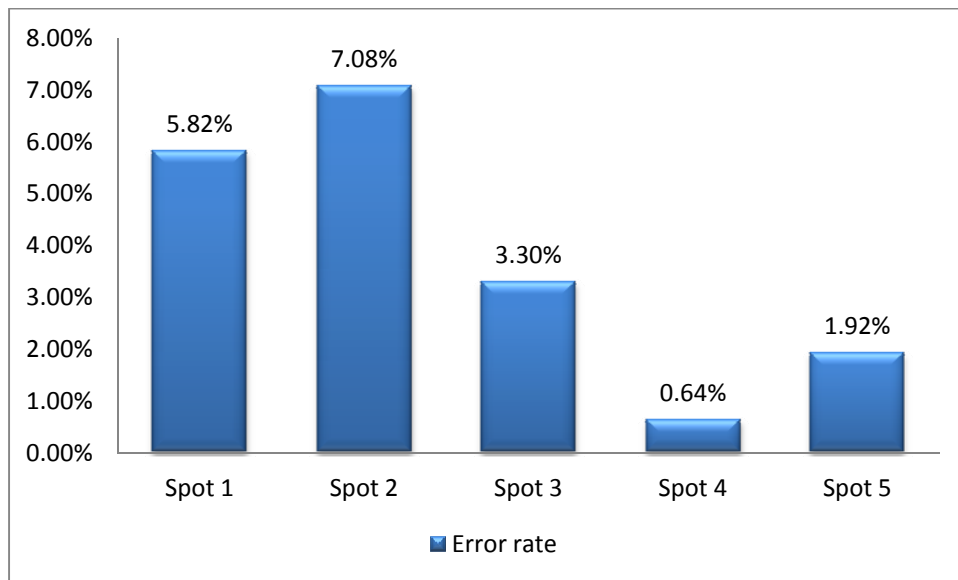


Figure 5-7 : Error Rates for Each spot

One of the main sources of error is signal blockage caused by presence of external objects between the sensor and collector. Having compared the false concealment error rate and false

detection error rate during the test in Figure 5-8, it is observed that false concealment error is dominant for four of the spots. So using repeaters in parking lots can decrease blocking and considerably increase the overall performance.

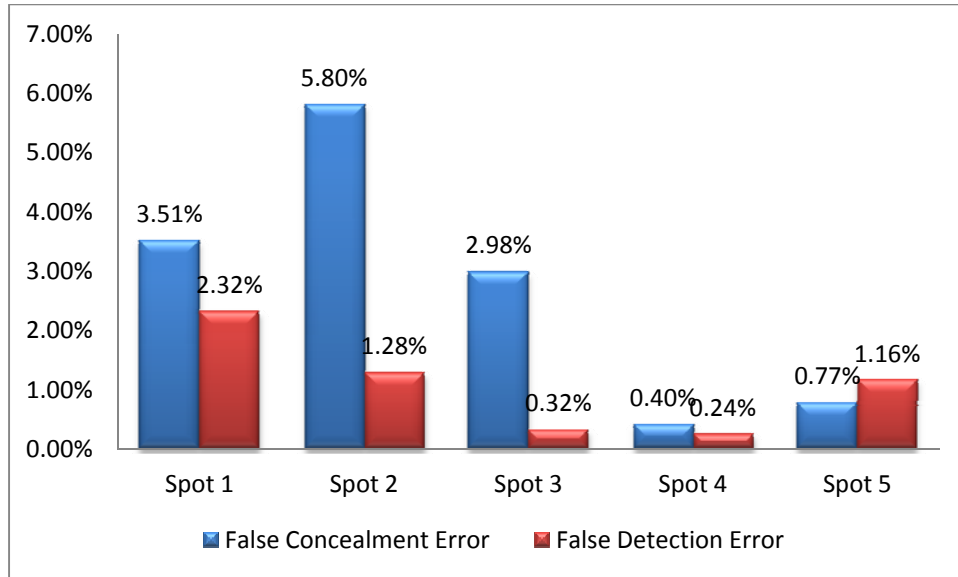


Figure 5-8: Ratio of different type of errors for each spot

One other interesting result during the experiment is the time distribution of parking events in each spot, which is a proxy for dynamics of events at different times of the day. As demonstrated in Figure 5-9, most of the events in the parking lot have occurred between 9 a.m. and 5 p.m.

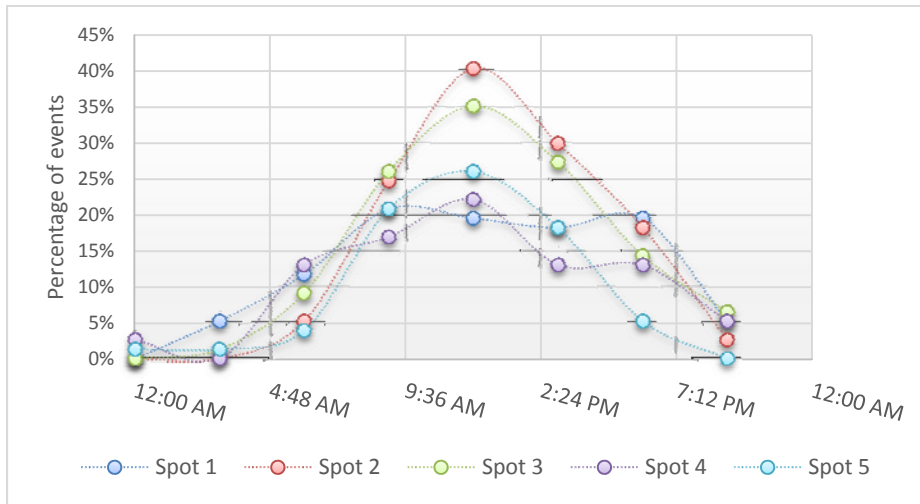


Figure 5-9: Distribution of events during the day

The distribution of average time which trucks stay at the parking in each time interval and occupancy of spot is also measured. As demonstrated in Figure 5-10, trucks that park in the evening occupy their spots for a much longer time. These trucks usually stay for the whole night at the truck parking areas.

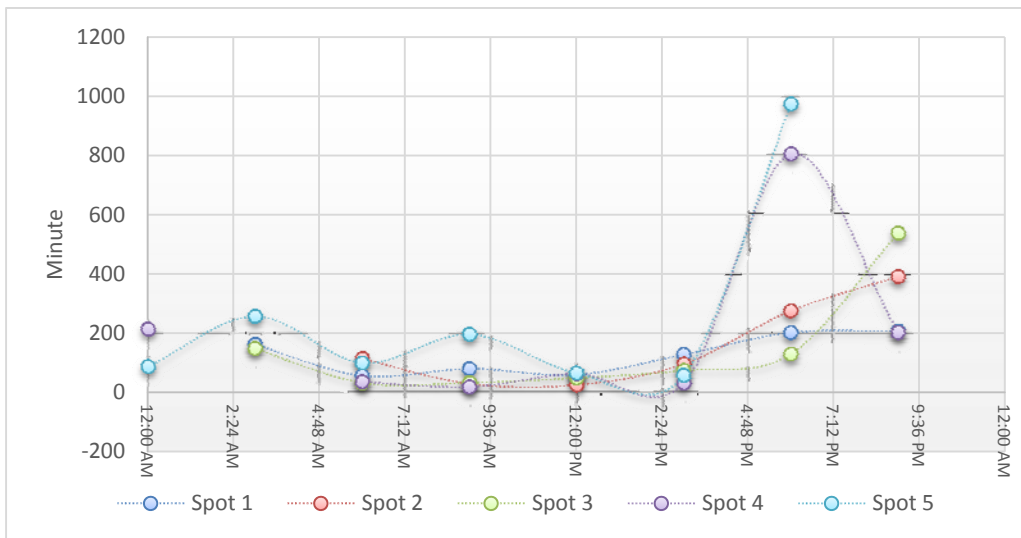


Figure 5-10: Distribution of average occupancy time during the day

To test the consistency of system's performance during the day, time distribution for the error rates of the system is calculated. As shown in Figure 5-11, error rates fluctuate over time but remain below 5 percent with an average of 3.75 percent.

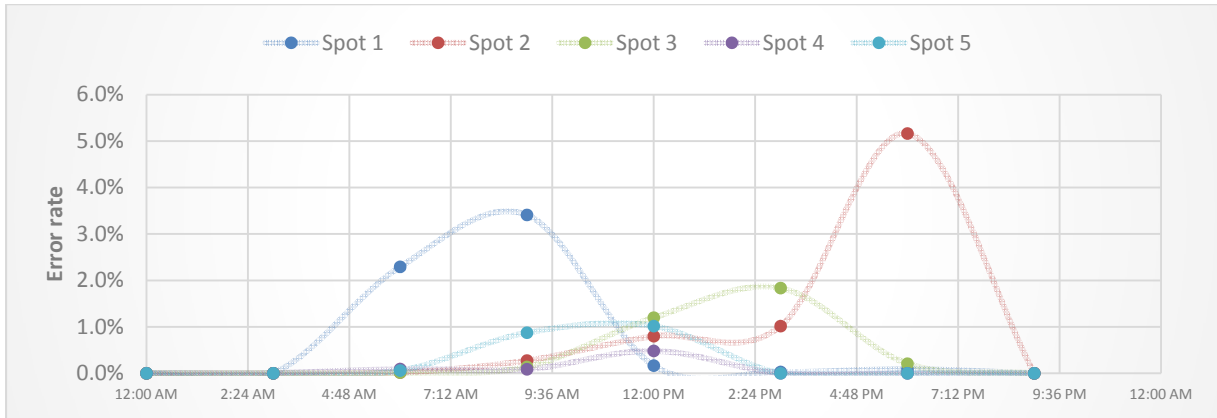


Figure 5-11: Distribution of error rates during the day

6 Conclusions

In this project, hardware and software components for a real-time truck parking information system were developed and tested. This system consists of a sensing component, a collecting component, a processing component and a user interface component. Among different types of common technologies for parking application, magnetic sensors were used for detecting vehicles due to their relative low cost. Both sensing and collecting components are enabled with IEEE 802.15.4 standard to form short-range wireless network architecture. The collecting component is also connected to data centers through cellular network. At the data center, using advanced algorithms, collected data is processed in real-time and updated information about the status of the parking spots is provided. User interfaces are designed to access the servers and to monitor the occupancy of parking spots.

With the help from SHA, the system has been tested and deployed at I-95 North Welcome Center. Using the results of the deployment, the system was modified and the collected data were processed at UMD campus's data center. After cross-checking the results with ground truth information provided by the system, performance of this system was measured. The overall error rate of the system was 3.75 percent on average, which means the system can provide accurate information on the status of parking spots 96.25 percent of the time. The error rate can potentially be lowered by using more sensors at each spot and using repeaters to avoid signal blockings. The accuracy and performance of the system can be customized for each facility based on their requirements and their budget limitations. Real-time access to the status of the spots can be disseminated to the drivers through different media. A TCP/IP enabled user interface software was developed in this project. All activities for each individual spot are stored

in a database. In addition to providing real-time parking availability to the truckers, analysis of historical data for each spot and for the parking lot as a whole can reveal dynamics of events and assist managers to make more informed decisions about regulations and operations of the facility. If all truck parking facilities in the area are equipped with such system, truckers can be directed to the next parking lots and utilization of all facilities can be optimized.

7 References

1. Study of Adequacy of Commercial Truck Parking Facilities –Technical Report, Publication FHWA-RD-01-158. Federal Highway Administration, U.S. Department of Transportation, March 2002
2. Commercial Driver Rest and Parking Requirements: Making Space for Safety, Report FHWA-MC-96-0010, FHWA, U.S. Department of Transportation, May 1996.
3. Fleming, G., “Truck Parking Partnership Study,” Baltimore Metropolitan Council, Final Report, October 2006
4. Rest Area Forum: Summary of Proceedings, Publication No. FHWA-RD-00-034, Federal Highway Administration, U.S. Department of Transportation, Washington, D.C., December 1999
5. National Transportation Safety Board, Truck Parking Areas, Report Number NTSB/SIR-00/01, Washington, D.C., May 2000.
6. Wegmann, F.J., A. Chatterjee, and D.B. Clarke, “Truck Parking at Night Along Interstate Highways—Tennessee Experience,” Proceedings, Second International Truck and Bus Safety Symposium, University of Tennessee Transportation Center, Knoxville, October 1999
7. Garber N.J., H. Wang and D. Charoenphol, “ESTIMATING THE SUPPLY AND DEMAND FOR COMMERCIAL HEAVY TRUCK PARKING ON INTERSTATE HIGHWAYS: A CASE STUDY OF I-81 IN VIRGINIA,” Virginia Transportation Research Council in Cooperation with the U.S. Department of Transportation and Federal Highway Administration, Final Report, VTRC 03-R4, December 2002
8. Trombly, J.W., “Dealing with Truck Parking Demands,” National Cooperative Highway Research Program, Synthesis 317, National Research Council, Washington, D.C., 2003
9. “Minnesota Interstate Truck Parking Study,” Minnesota Department of Transportation, January 2008

10. Heinitz, F. M. and N. Hesse, "Estimating Time-Dependent Demand for Truck Parking Facilities Along a Federal Highway," *Transportation Research Record: Journal of the Transportation Research Board*, No. 2097, National Academies, Washington, D.C., 2009, pp. 26–34.
11. Maryland Department of Transportation, "Maryland Truck Parking Study," Federal Highway Administration, U.S. Department of Transportation, 2005
12. Rodier, C. J., S. A. Shaheen, "Commercial Vehicle Parking In California: Exploratory Evaluation of the Problem and Possible Technology-Based Solutions," California PATH Research Report, UCB-ITS-PRR-2007-11, 2007
13. Adams, B. T., P. Srivastava, B. Wang, and L. Ogard, "LOW COST STRATEGIES FOR SHORT TERM PARKING ON INTERSTATE HIGHWAYS OF THE MVFC," National Center for Freight & Infrastructure Research & Education, College of Engineering, Department of Civil and Environmental Engineering, University of Wisconsin, Madison, Project MVFC 04, 2009
14. Bronzini, M., R. Gomez, A. Choudhary, "Feasibility of Using Remote Sensing to Monitor Truck Rest Area Availability and Utilization," George Mason University, Fairfax, VA
15. "SmartPark Real-Time Parking Information for Truckers," U.S. Department of Transportation, Federal Motor Carrier Safety Administration, Technology Division, (<http://www.fmcsa.dot.gov/facts-research/art-technology-SmartPark-Real Time.htm>)
16. Farshad Ahdi, Mehdi Kalantari Khandani, Masoud Hamedi, Ali Haghani, "Traffic Data Collection and Anonymous Vehicle Detection Using Wireless Sensor Networks", Project Number SP009B4H Final Report, Maryland State Highway Administration, May 2012.